Chapter 5

Nonlinear generation of modes on a symmetrically kinked bar.

The situation to be studied in this chapter, a bar kinked symmetrically at points B and B′ and rigidly clamped at its extreme ends, C and C′, is shown schematically in Fig.5.1. We concentrate our attention on symmetric modes to reduce the algebra - antisymmetric modes can be treated similarly and there is no coupling between the two classes.

5.1 Linear analysis.

As our method of analysis looks at the effect of nonlinear forces on the linear modes of a bar, it is necessary first to calculate the linear solution to the equation of motion of the bar. In the simplest linear approximation, the equation of motion for any straight section of bar may be written

$$\rho\frac{\partial^2\xi}{\partial t^2} = -E\kappa^2\frac{\partial^4\xi}{\partial x^4} + \frac{T_1}{S}\frac{\partial^2\xi}{\partial x^2} - D\frac{\partial\xi}{\partial t} \tag{5.1}$$

where ξ is the normal displacement, ρ is the density of the material, S is the cross-sectional area, κ is the radius of gyration, E is Young's Modulus, D is a measure of damping and T_1 is the tension in the bar. Adopting this co-ordinate system for the section AB of the bar with length L, a simple change of notation gives the equation of motion for the bent end BC with length l,

$$\rho\frac{\partial^2\zeta}{\partial t^2} = -E\kappa^2\frac{\partial^4\zeta}{\partial y^4} + \frac{T_2}{S}\frac{\partial^2\zeta}{\partial y^2} - D\frac{\partial\zeta}{\partial t} \tag{5.2}$$

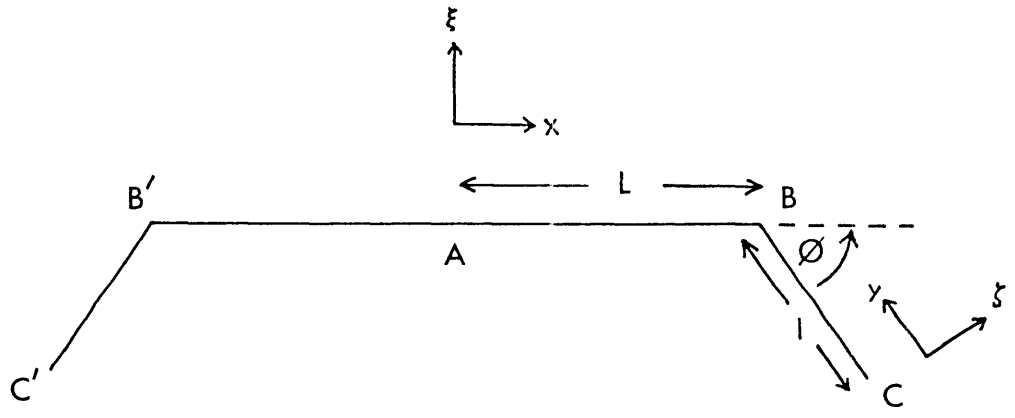

Figure 5.1: The kinked bar and its coordinate system.

where ζ is the normal displacement and T_2 is the tension along this section. The co-ordinates are defined in Fig. 5.1.

For simplicity we will consider only modes symmetric about the midpoint of the bar. Symmetry then requires the following conditions at point A:

$$\frac{\partial \xi}{\partial x} = 0, \qquad \frac{\partial^3 \xi}{\partial x^3} = 0 \qquad \text{at } x = 0. \tag{5.3}$$

The solution to equation (5.1) is therefore

$$\xi_n(x) = [a_n \cos \alpha_n x + b_n \cosh \alpha_n x] \sin(\omega_n t + \phi_n) \exp(\frac{-t}{\tau_n}) \tag{5.4}$$

where a_n and b_n are constants dependent only on further matching conditions at point B, ω_n is the mode frequency, and τ_n is derived from the damping coefficient D. Boundary conditions at the clamped end C, namely

$$\zeta = 0 \qquad \text{and} \qquad \frac{\partial \zeta}{\partial y} = 0 \qquad \text{at } y = 0 \tag{5.5}$$

give the solution to the equation (5.2) as

$$\zeta(y) = \left[a_n'(\sin \alpha_n y - \sinh \alpha_n y) + b_n'(\cos \alpha_n y - \cosh \alpha_n y)\right] \sin(\omega_n t + \phi_n) \exp(\frac{-t}{\tau_n}) \tag{5.6}$$

where again the constants a_n' and b_n' depend on matching conditions at point B. We assume for the linear approximation that $T_1 = T_2 = 0$ so that in both equations (5.4) and (5.6),

$$\alpha_n = \left[\frac{\omega_n^2 \rho}{E\kappa^2}\right]^{\frac{1}{4}} . \tag{5.7}$$

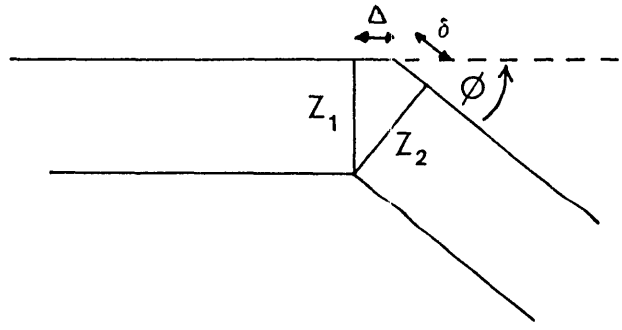

Figure 5.2: Second-order displacements at the kink.Δ and δ are positive and z_1, z_2 negative as drawn.

Matching conditions at the point B can now be used to determine the relation between a_n, b_n and a_n', b_n' and also the mode frequency ω and decay time τ_n . For continuity at B we must equate the components of displacement and write quite generally, as illustrated in Fig. 5.2, with z_1, z_2 for $\xi(L), \zeta(l)$ respectively, these quantities being negative as drawn,

$$\begin{aligned} z_1 &= -\delta \sin\phi + z_2 \cos\phi \\ -\Delta &= +\delta \cos\phi + z_2 \sin\phi \end{aligned} \tag{5.8}$$

where Δ and δ are the displacements parallel to the x and y axes respectively, arising out of second order changes in length of the bar and may therefore be equated to zero in first order. This reduces (5.8) to

$$z_1 = z_2 \cos\phi \quad \text{and} \quad 0 = z_2 \sin\phi \tag{5.9}$$

so that, provided $\phi \neq 0$, then $z_1 = z_2 = 0$ and point B remains fixed. Furthermore since bending moments at B must be finite and continuous,

$$\left.\frac{\partial \xi}{\partial x}\right|_{x=L} = -\left.\frac{\partial \zeta}{\partial y}\right|_{y=l} \tag{5.10}$$

and

$$\left.\frac{\partial^2 \xi}{\partial x^2}\right|_{x=L} = \left.\frac{\partial^2 \zeta}{\partial y^2}\right|_{y=l} . \tag{5.11}$$

These conditions then relate a_n, b_n, a_n' and b_n' and produce an equation relating the frequencies ω_n of the vibrational modes to the lengths L and l of the bar sections,

$$\left[\sin\alpha_n L + \cos\alpha_n L \frac{\sinh\alpha_n L}{\cosh\alpha_n L}\right]\left[\frac{\cos\alpha_n l \sinh\alpha_n l - \sin\alpha_n l \cosh\alpha_n l}{1 - \cos\alpha_n l \cosh\alpha_n l}\right] - 2\cos\alpha_n L = 0. \tag{5.12}$$

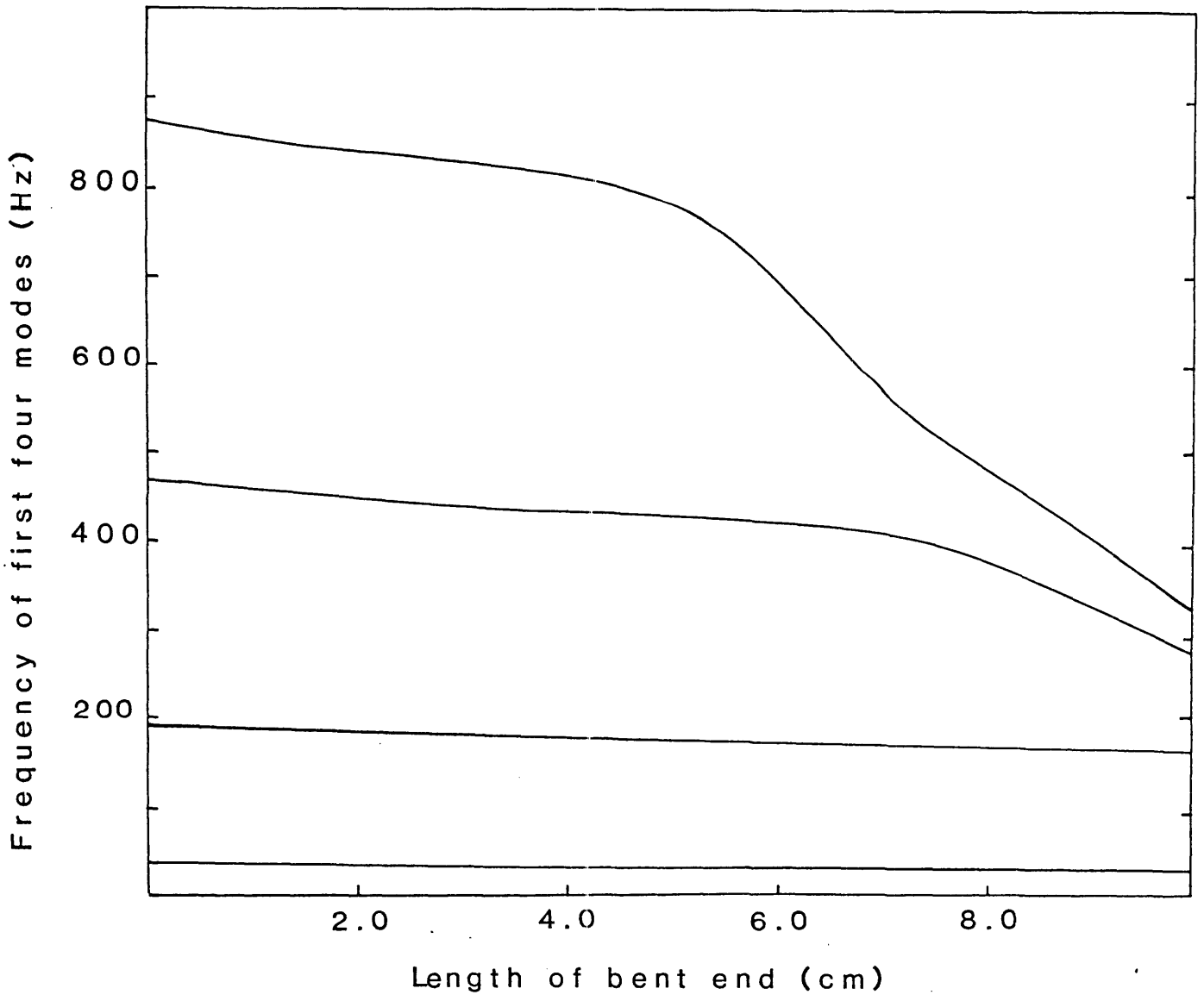

Figure 5.3: Fequencies of the symmetric modes of a kinked bar with central length 30cm and thickness 0.6mm as the length l of the clamped end sections is varied.

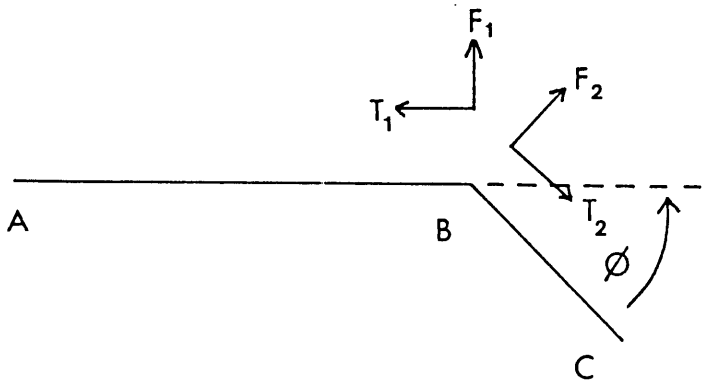

Figure 5.4: Force balance at the kink.

Fig. 5.3 is a plot of the variation of the frequencies of the first four symmetric modes with the length l of the section BC while L, the length of section AB, remains constant.

5.2 Nonlinear forcing terms.

As suggested earlier,there are two separate nonlinear forcing terms to be considered. The first, and as it turns out the more important one, arises from the coupling of tension and shear forces of the bar sections. Fig. 5.4 shows the shear and tensile forces present on the bar sections AB and BC. Balance of forces at the bend B requires

$$F_1 + F_2 \cos\phi - T_2 \sin\phi = 0 \tag{5.13}$$

$$T_1 - F_2 \sin\phi - T_2 \cos\phi = 0 \tag{5.14}$$

which in turn leads to

$$T_1 = \frac{F_1 \cos\phi + F_2}{\sin\phi} \tag{5.15}$$

$$T_2 = \frac{F_1 - F_2 \cos\phi}{\sin\phi} \quad . \tag{5.16}$$

Since F_1 and F_2 are shear forces at point B, they may be written

$$F_1 = -ES\kappa^2 \frac{\partial^3 \zeta}{\partial x^3}\bigg|_{x=L} \tag{5.17}$$

$$F_2 = -ES\kappa^2 \frac{\partial^3 \zeta}{\partial y^3}\bigg|_{y=l} \tag{5.18}$$

where we use the approximation that ξ and ζ are the linear modes previously derived. It is clear from equations (5.15)-(5.18) that T_1 and T_2 are of first order in ξ and ζ ; however their inclusion in equations (5.1) and (5.2) is such that the forcing terms $T_1\frac{\partial^2\xi}{\partial x^2}$ and $T_2\frac{\partial^2\zeta}{\partial y^2}$ are second order. For a single mode (ξ,ζ) of frequency ω on the bar, it is clear from (5.15) and (5.16) taken with (5.17) and (5.18), that these forcing terms have frequency 2ω.

The second nonlinearity to be considered arises from the unbalanced moments around point B. This time the nonlinear driving mechanism is derived independently of the linear modes and applied later to the linear solution. Equations (5.1), (5.2), (5.4), and (5.6) still hold but the boundary conditions at point B are now written as the full equations (5.8) to include the second-order change in length of the bar that was neglected in the linear case. These length changes are given by

$$\Delta = \int_0^L \left[1 + \left(\frac{\partial\xi}{\partial x}\right)^2\right]^{\frac{1}{2}} dx - L \tag{5.19}$$

for section AB and

$$\delta = \int_0^l \left[1 + \left(\frac{\partial\zeta}{\partial y}\right)^2\right]^{\frac{1}{2}} dy - l \tag{5.20}$$

for BC. Thus for a bar vibrating with frequency ω, point B undergoes both a static and an oscillatory (2ω) displacement. Fig. 5.2 illustrates the oscillatory displacement around the static displacement of B. We may neglect the static displacement as it is not significant in our investigations, so that we write the nonlinear displacements $\xi'_{2\omega}$ and $\zeta'_{2\omega}$ as

$$\xi'_{2\omega} = z_1(x)\cos 2\omega t \tag{5.21}$$

and

$$\zeta'_{2\omega} = z_2(y)\cos 2\omega t. \tag{5.22}$$

It should be noted that $\xi'_{2\omega}$ and $\zeta'_{2\omega}$ are solutions to equations (5.1) and (5.2) but with different matching conditions at point B from the linear solutions. Hence, neglecting damping, we may write

$$z_1(x) = e\cos\alpha_2 x + f\cosh\alpha_2 x \tag{5.23}$$

$$z_2(y) = e'(\sin\alpha_2 y - \sinh\alpha_2 y) + f'(\cos\alpha_2 y - cosh\alpha_2 y) \quad . \tag{5.24}$$

As we have said, point B may no longer be taken to be fixed as in the linear case. However we will approximate by assuming that the angle ϕ remains unchanged and that there are

no linear modes of frequency 2ω initially present. For the linear modes we would have had

$$\xi(L) = \zeta(l) = 0$$
$$\left.\frac{\partial \xi}{\partial x}\right|_{x=L} = -\left.\frac{\partial \zeta}{\partial y}\right|_{y=l} \tag{5.25}$$

whereas for the nonlinear modes, to a first approximation,

$$\left.\frac{\partial \xi}{\partial x}\right|_{x=L} = 0 \qquad\qquad \left.\frac{\partial \zeta}{\partial y}\right|_{y=l} = 0. \tag{5.26}$$

Equation (5.26) relates ϵ to f and ϵ' to f'. Furthermore the geometry of Fig. 5.2 gives, at point B, since z_1 and z_2 as drawn are negative,

$$z_1 = -\delta \sin\phi + z_2 \cos\phi \tag{5.27}$$
$$z_2 = -\Delta \sin\phi + z_1 \cos\phi \quad . \tag{5.28}$$

Together with equations (5.21)-(5.24) we now have sufficient conditions to express the amplitude e of the nonlinear 2ω mode in terms of the amplitude a of the linear ω mode initially present on the bar.

The forcing mechanism at point B that we are considering at present is the result of unbalanced bending moments M_1 and M_2 on the two sections of the bar, where

$$M_1 = -ES\kappa^2 \frac{\partial^2 \xi'_{2\omega}}{\partial x^2} \tag{5.29}$$

and

$$M_2 = -ES\kappa^2 \frac{\partial^2 \zeta'_{2\omega}}{\partial y^2} \quad . \tag{5.30}$$

The total unbalanced moment $M = M_1 - M_2$ then appears as a driving term in equations (5.1) and (5.2) of the form

$$M \frac{d}{dx}\delta(x - L) \tag{5.31}$$
$$M \frac{d}{dy}\delta(y - l) \tag{5.32}$$

where $\delta(x)$ is the Dirac delta function. The frequency of this driving term is once again 2ω.

The length changes Δ and δ of equation (5.19) and (5.20) lead to a further nonlinearity which we should point out, though we will not investigate it in detail. As well as a concentrated moment of frequency 2ω at the kink, these contractions give rise to tension forces T'_1 and T'_2 in the two parts of the bar, also at frequency 2ω. Indeed the tension T'_1 would be

present for the same reason in a straight bar with rigidly clamped ends. The driving term arising from this tension has the form

$$T_1' \frac{\partial^2 \xi}{\partial x^2} \qquad\qquad T_2' \frac{\partial^2 \zeta}{\partial y^2} \tag{5.33}$$

and is of third order and frequency 3ω. Its importance can be expected to be less than that of second order terms at frequency 2ω already discussed.

5.3 Solution.

The equations of motion (5.1) and (5.2) must now be modified to include the nonlinear forcing terms specifically. To do this we suppose that $u_n(t)\psi_n(x)$ represents the normal modes over the whole range of x from 0 to $L + l$, with $\psi_n(x) = \xi(x)$ for $0 \leq x \leq L$ and $\psi_n(x) = \zeta(L + l - x)$ for $L \leq x \leq L + l$. Let us further suppose that the ψ_n are normalized over this whole range - they are of course orthogonal. Now we want to examine the behaviour of mode p of frequency ω_p and small amplitude in the presence of a large-amplitude mode m, where $\omega_p \approx 2\omega_m$. Equations (5.1) and (5.2) for mode p can be written in combination as

$$\rho\psi_p \frac{d^2 u_p}{dt^2} = -E\kappa^2 u_p \frac{d^4 \psi_p}{dx^4} - D\psi_p \frac{du_p}{dt} + \frac{T(m)}{S} u_m \frac{d^2 \psi_m}{dx^2} + M(2m)\frac{d}{dx}\delta(x - L) \tag{5.34}$$

where $T(m) = T_1$ for $0 \leq x \leq L$ and T_2 for $L \leq x \leq L + l$. $T(m)$ and u_m vary with frequency ω_m and $M(2m)$ with frequency $2\omega_m$.

Now we multiply both sides of (5.34) by $\psi_p(x)$ and integrate over $0 \leq x \leq L + l$, remembering the orthonormality, to get

$$\frac{d^2 u_p}{dt^2} + \omega_p^2 u_p = -\frac{D}{\rho}\frac{du_p}{dt} + \frac{u_m}{\rho S}\left[T_1(m)I_1 + T_2(m)I_2\right] + \frac{M(2m)}{\rho}\left.\frac{d\psi_p}{dx}\right|_{x=L} \tag{5.35}$$

where

$$I_1 = \int_0^L \psi_p(x)\frac{d^2\psi_m(x)}{dx^2}\,dx \qquad\qquad I_2 = \int_L^{L+l} \psi_p(x)\frac{d^2\psi_m(x)}{dx^2}\,dx \tag{5.36}$$

The second and third terms on the right side of (5.35) are forcing terms, both with frequency $2\omega_m$.

The relative importance of the contribution made by the tension terms T and moment term M in (5.35) is not immediately clear and may vary from case to case. For the relatively thin bar examined in our experiment, theory suggests that the tension terms are clearly dominant and indeed the moment term is so small it can be neglected.

If we had been interested in the third order 3ω terms set out in (5.35) then these would enter (5.35) similarly as $[T_1' I_1 + T_2' I_2]$. Since the integral I_1 does not vanish even for a rigidly clamped bar, this mode coupling mechanism is always present. This is in counter-distinction from the case of a rigidly supported string, for which the equivalent integral vanishes identically.

The differential equation (5.36) for the p^{th} mode has the general form

$$\frac{d^2 u_p}{dt^2} + \omega_p^2 u_p = g(t) \tag{5.37}$$

where g contains both damping and forcing terms. If we write

$$u_p = a_p \sin(\omega_p t + \theta_p) \tag{5.38}$$

where both a_p and $\theta_p$are slowly varying functions of time, then (5.36) is in the standard form for treatment by the method of slowly varying parameters. The procedure is now analogous to that used in our previous analysis of the string and the resulting equations are

$$\langle \dot{a_p} \rangle = \beta_m a_m^2 \cos[(2\omega_m - \omega_p)t + 2\theta_m - \theta_p] - \frac{a_p}{\tau_p} \tag{5.39}$$

and

$$\langle \dot{\theta_p} \rangle = \beta_m \frac{a_m^2}{a_p} \sin[(2\omega_m - \omega_p)t + 2\theta_m - \theta_p] \tag{5.40}$$

where the mode coupling coefficient

$$\beta_m = -\frac{T_1^{(a)} \alpha_m^2 I_1}{4\rho S \omega_p} + \frac{T_2^{(a)} \alpha_m^2 I_2}{4\rho S \omega_p} \tag{5.41}$$

follows from (5.35) and we have assumed that $\omega_p \approx 2\omega_m$. $T_1^{(a)}$ and $T_2^{(a)}$ represent the tension terms from (5.15) and (5.16) divided by the time-dependent amplitude of motion.

Since all that is driving mode p assuming it to start from zero amplitude, is the second harmonic of mode m, and since we assume $a_m \gg a_p$, we can write

$$\theta_m = \text{const.} \qquad \dot{\theta_p} = 2\omega_m - \omega_p \tag{5.42}$$

and then (5.40) gives

$$2\omega_m - \omega_p = \beta_m \frac{a_m^2}{a_p} \sin(2\theta_m - \theta_p^0) \tag{5.43}$$

where θ_p^0 is the value of θ_p at $t = 0$. Inserting (5.42) and (5.43) in (5.39) then gives

$$\langle \dot{a} \rangle = \beta_m a_m^2 \left\{ 1 - \frac{(2\omega_m - \omega_p)^2 a_p^2}{\beta_m^2 a_m^4} \right\}^{\frac{1}{2}} - \frac{a_p}{\tau_p} \quad . \tag{5.44}$$

Clearly the rate of increase of a_p is greatest if the resonant condition $\omega_p = 2\omega_m$ is closely satisfied, as indeed we should expect.

In the experiment to be described, the amplitude of mode m is initially large and then decays exponentially, while the amplitude of mode p is initially near zero. Equation (5.44) predicts that a_p will rise to a maximum, which depends on the behaviour of a_m , and then decay towards zero.

This behaviour can be made explicit for the simple case in which the decay times τ_m and τ_p are constants and ω_p is exactly equal to $2\omega_m$. Integration of equation (5.44) for the case of no initial excitation of mode p then gives

$$a_p(t) = \beta_m a_m^{0\,2} \left[\frac{\tau_m \tau_p}{\tau_m - 2\tau_p}\right] \left[\exp(\frac{-2t}{\tau_m}) - \exp(\frac{-t}{\tau_p})\right] \qquad (5.45)$$

where a_m^0 is the initial amplitude of mode m. In the more general case, integration of (5.40) and (5.44) can give beatlike phenomena superposed on a curve of the same general shape as given by (5.45).

Another simple case that can be solved explicitly is that of continuous excitation of mode m to amplitude a_m^0 . This is equivalent to letting $\tau_m \rightarrow \infty$, so that

$$a_p(t) = \beta_m a_m^{0\,2} \tau_p \left(1 - \exp(\frac{-t}{\tau_p})\right) \quad . \qquad (5.46)$$

5.4 Admittance of the bar.

Since mode conversion is significant only when one normal mode has nearly twice the frequency of another, the dimensions of the bar are important. Choosing for our experiment a galvanised steel bar of thickness 0.6mm, and length 30cm between B and B′ (refer to Fig. 5.1), the length of the ends B C and B′C′ necessary to achieve an appropriate resonance can be calculated. Fig. 5.3 shows how the resonant frequencies of the symmetric modes vary with change in length of the bent ends. The figure shows us that for such a bar, if the bent ends are about 9cm in length, then the third symmetric mode (ω_3) will have twice the frequency of the second symmetric mode (ω_2).

A bar of these dimensions was clamped between two tilting vises and the admittance characteristic at its centre point A determined with a Bruel & Kjaer impedance head type 8001 in conjunction with an integrator and a dual channel FFT spectrum analyzer (see Fig.5.5). The length of the bent ends was varied until ω_3 was closely equal to $2\omega_2$, the

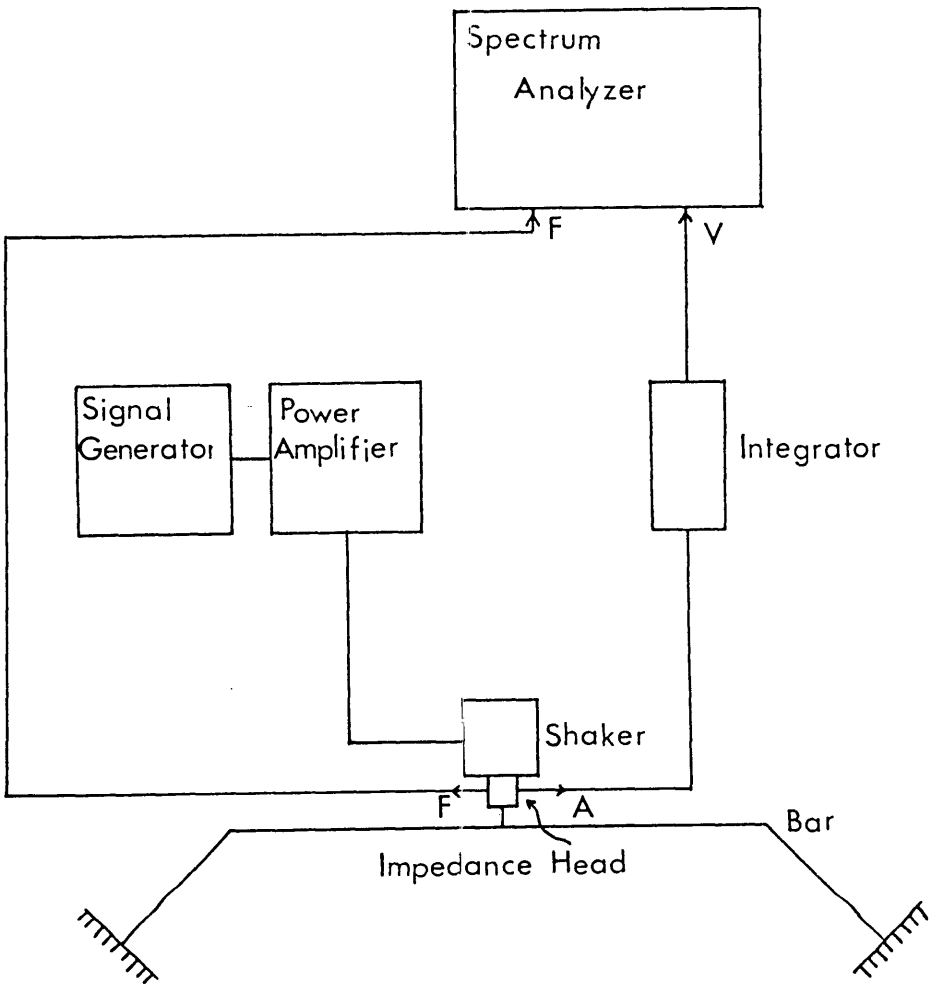

Figure 5.5: Experimental arrangement to measure the admittance of the clamped kinked bar.

final length being approximately 8.8cm. The admittance curve measured is shown in Fig. 5.6 together with the admittance calculated for such a bar using the linear theory and neglecting damping.

It is worth noting here the shape of the admittance curve in as much as the whole curve appears raised for lower frequencies. While this may seem slightly surprising at first it is quite simply explained by considering the characteristic admittance of a bar vibrating such that its motion is primarily one of bending (Skudrzyk 1968). Like that of the string the admittance of the bar is inversely proportional to the phase velocity c but unlike the string the velocity for a bar is not independent of the frequency, varying instead like $\sqrt{\omega}$ (as shown in chapter 4). Hence the raising of the admittance curve for smaller values of ω .

5.5 Preliminary experiments.

The mode shapes for ω_2 and ω_3 were measured, again using a shaker at the centre of the bar but this time the bar was shaken with a frequency equal to the resonant frequency ω_2 . A Bruel & Kjaer subminiature accelerometer was moved along the bar at 1cm intervals between the centre and one end. The signal was fed via an amplifier through an appropriate filter so that the amplitudes of the second and third modes could be measured on an oscilloscope screen. Fig 5.7 shows the results. The measurements were then repeated for the third mode alone while the bar was shaken at a frequency equal to ω_3 and the same mode shape was observed. Incidently, we can see that, provided the shaker had negligible amount of ω_3 on its waveform while vibrating with frequency ω_2 , the amplitude of the third mode generated by the second is quite significant.

The mode shapes enabled us to determine appropriate points to pluck, hammer or shake the bar in subsequent experiments in order that we should have particular proportions of ω_2 and ω_3 initially present.

5.6 Damping.

A measurement of the free decay of each mode was necessary for quantitative comparison of theoretical and experimental results. The decay of the second mode was measured by plucking the bar close to the centre so that it had significant amplitude which was then observed, as it decayed , on a storage oscilloscope. The experiment was repeated for the

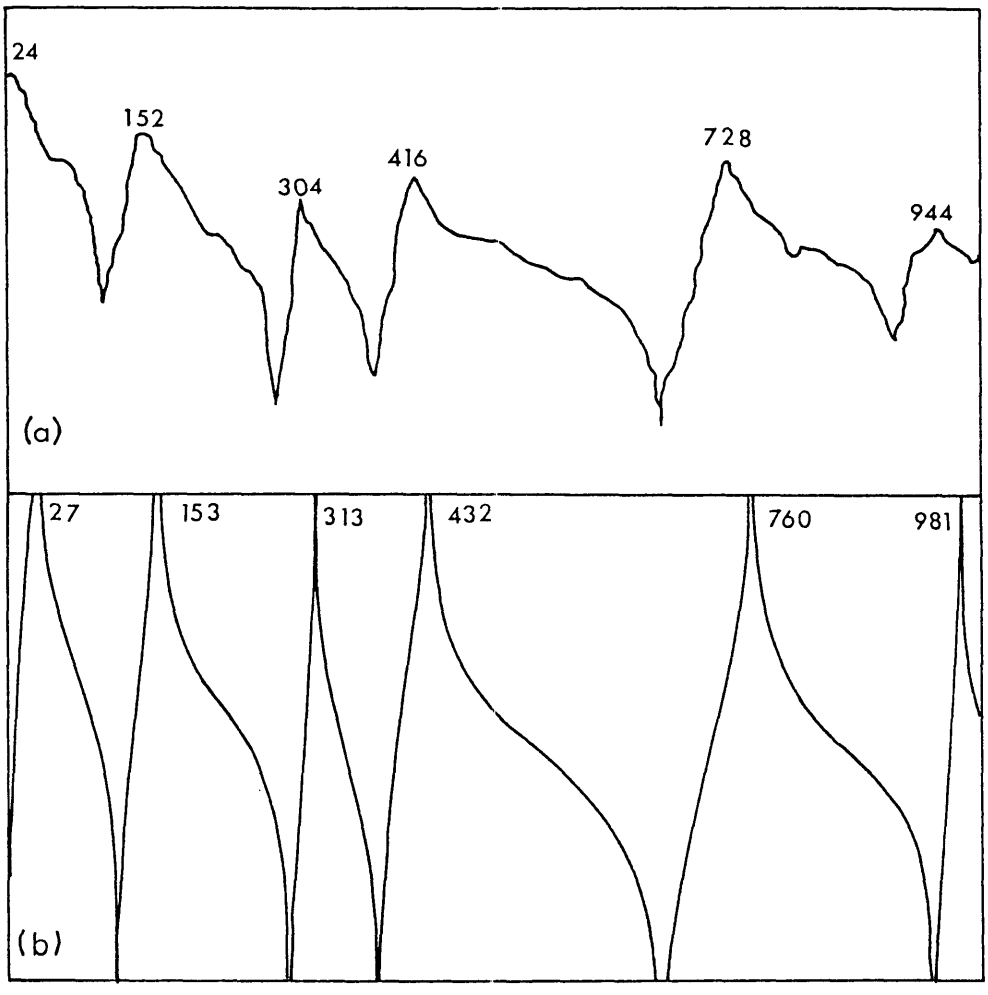

Figure 5.6: Mechanical admittance at the centre point A of a symmetrically kinked bar (a) as measured and (b) as calculated.

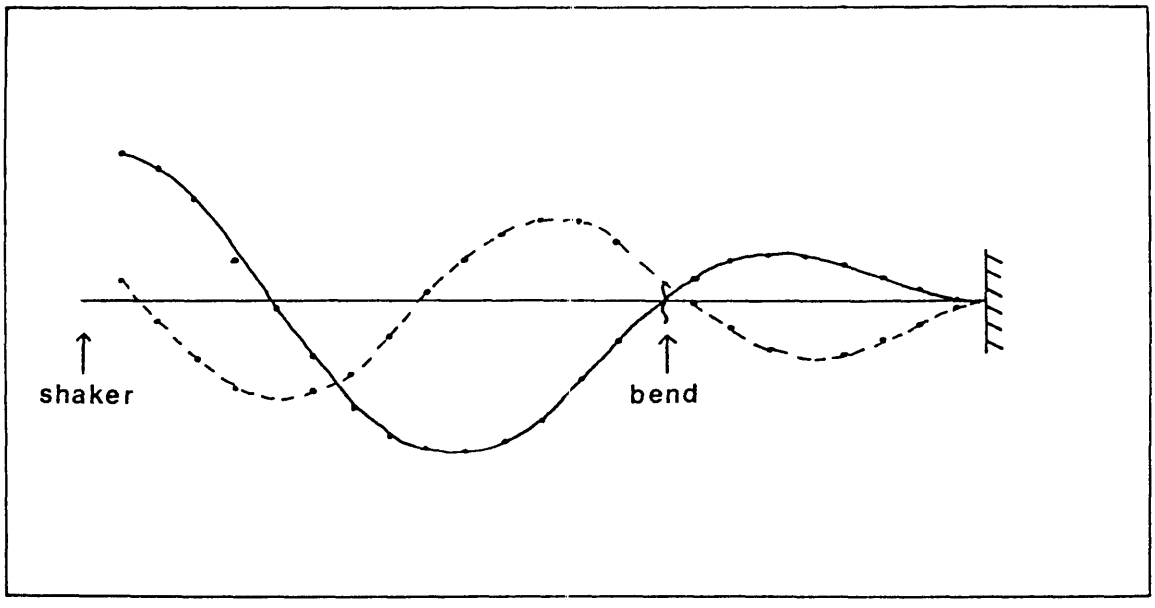

Figure 5.7: Mode shapes for the second and third modes when the bar was shaken at ω_2.

measurement of the decay of mode three, this time the bar was plucked close to the bend so that the proportion of mode three compared with the lower modes was at least as large as possible.

The results showed that while the second mode decayed exponentially with time such that τ_2=0.26 s, the decay time for the third mode appeared to change with amplitude, becoming longer for smaller amplitude. Clearly, with several modes present on the bar we must expect interaction terms that will affect the apparent damping. Our investigations are not however concerned with the exact damping behaviour of the bar and so we considered it adequate to take as an average decay rate for the third mode, of τ_3=0.25 s.

5.7 Measurements of nonlinear generation.

The first real check for the behaviour described in (5.44) was to shake the bar, at a frequency equal to ω_2 , on a node of the third mode, using a subminature accelerometer positioned at the centre point A of the bar to measure the amount of third mode generated. Positioning of the shaker on this mode was to ensure that any ω_3 component present as distortion in the shaker output was of negligible consequence to the result. It served the purpose of ensuring that the only point "clamped" into vibrating at ω_2 only by the presence of the shaker, was

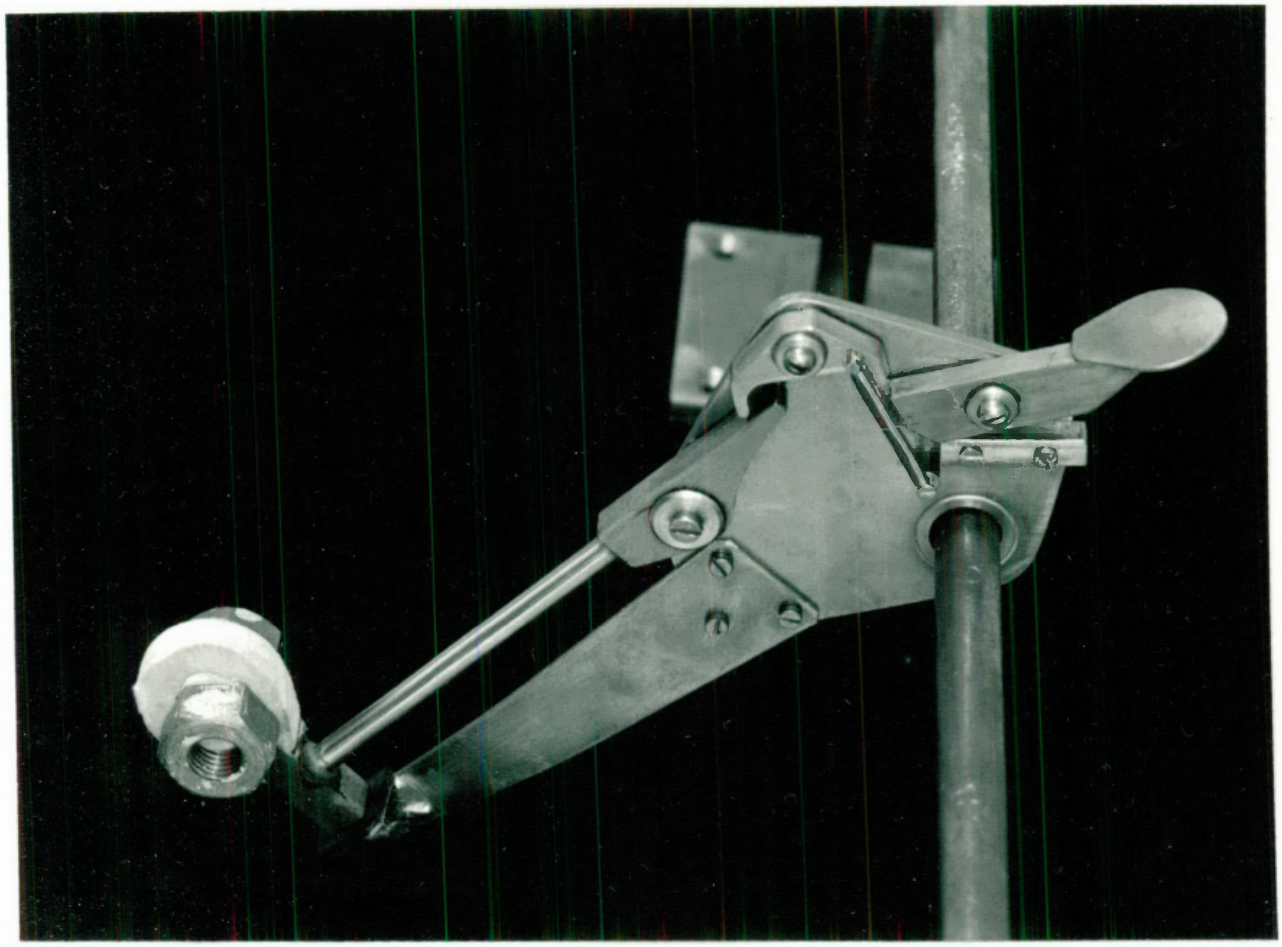

Figure 5.8: Weighted piano hammer used to strike the bar.

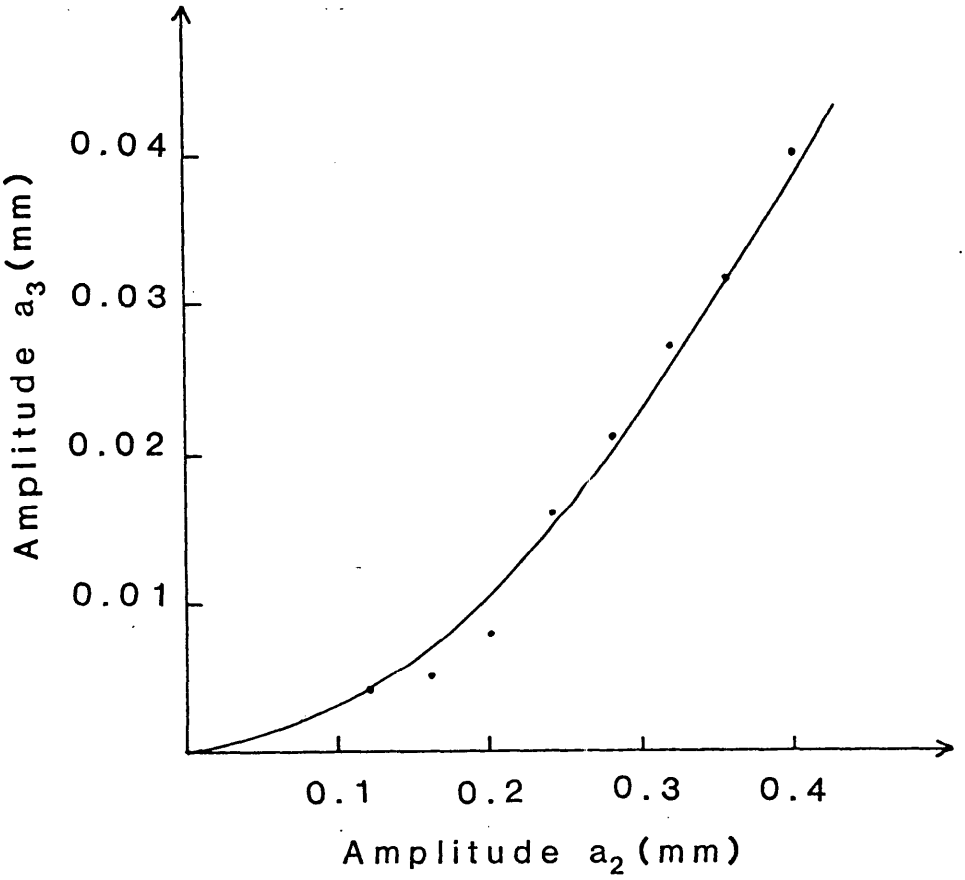

Figure 5.9: Measured amplitude a_3 of the third mode as a function of the amplitude a_2 of the second mode for a kinked bar shaken at the node of the third mode. The curve is a_3=const. x a_2^2.

a node of ω_3 .

The result of this measurement is shown in Fig. 5.9 and has the form

$$a_3 = 250a_2^2 \tag{5.47}$$

where a_2 and a_3 are both measured in metres. This agrees with the limiting form of equation (5.46) as $t \rightarrow 0$. As we discuss in a moment, the bar has a value of τ_3 equal to about 0.25s so that we conclude that the coupling coefficient β_2 has a value of about 1000 $m^{-1}s^{-1}$ for this particular bar. The actual value calculated from the rather involved expression in equations (5.35) and (5.36) was about 2560 $m^{-1}s^{-1}$. In view of the approximations involved and the significant effects of minor departures from the condition $\omega_3 = 2\omega_2$ as shown by (5.44), this result represents moderately satisfactory agreement.

The theory was further examined in a second experiment, in which the bar was struck with a weighted piano hammer (Fig. 5.8) on a node of the third mode, the objective being to excite the bar into a vibration that initially excluded this mode and to observe the modes subsequent amplitude. The vibration signal from a subminiature accelerometer, positioned as before at the centre of the bar, was recorded on a Nagra IV tape recorder and later analysed with an appropriate filter to determine the time behaviour of both the second and third modes. The analysis showed that the second mode decayed more or less exponentially in time with τ_2=0.26 s while the third mode grew from near zero to a maximum in a time of order 0.1 s before decaying slowly to zero. A typical trace is shown in Fig. 5.10. The peak amplitude reached by the missing third mode, and the time between the hammer blow and this peak, were both plotted as functions of a_2, the initial amplitude of the second mode. These measurements are shown in Fig. 5.12 along with the behaviour predicted by theory.

Fig. 5.11 shows the calculated behaviour of the third mode amplitude when the bar is hit so as to make its initial value zero. Comparison with Fig. 5.10 shows that the general predictions of the theory are qualitatively similar to the experimental behaviour.

For a more quantitative assessment of the theory we must turn to Fig. 5.12 which shows the predicted maximum amplitude and time to reach that amplitude plotted alongside the experimental data. It must be noted however that the theory relies on the measurement of the decay constants τ_2 and τ_3 and that while the second mode decayed exponentially with time, the decay time of the third mode, as we noted earlier, appeared to change with amplitude. The approximation involved here may describe in part the small descrepencies between theory and experiment shown in Figs. 5.10 - 5.12.

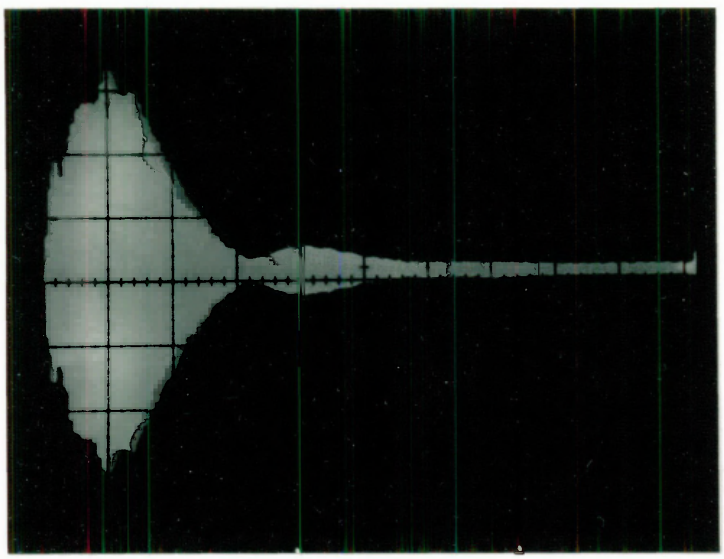

Figure 5.10: Oscilloscope trace of the behaviour of the third mode amplitude with time when a kinked bar is excited by a hammer blow close to a node for this mode. Total tracelength is 1 s.

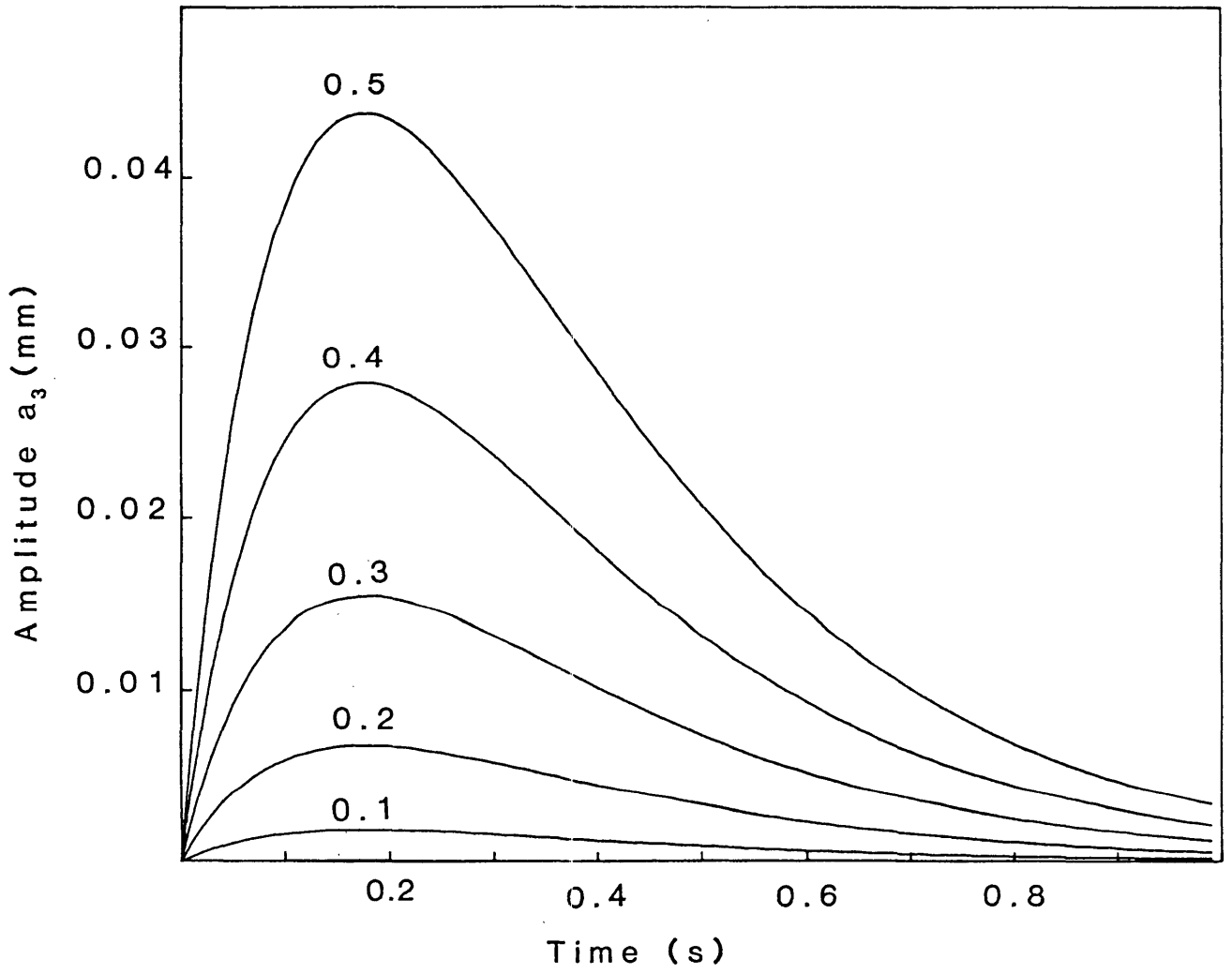

Figure 5.11: Calculated behaviour of the third mode amplitude a_3 as a function of time for different initial amplitudes of the second mode excitation (shown as a parameter), with simple linear damping assumed.

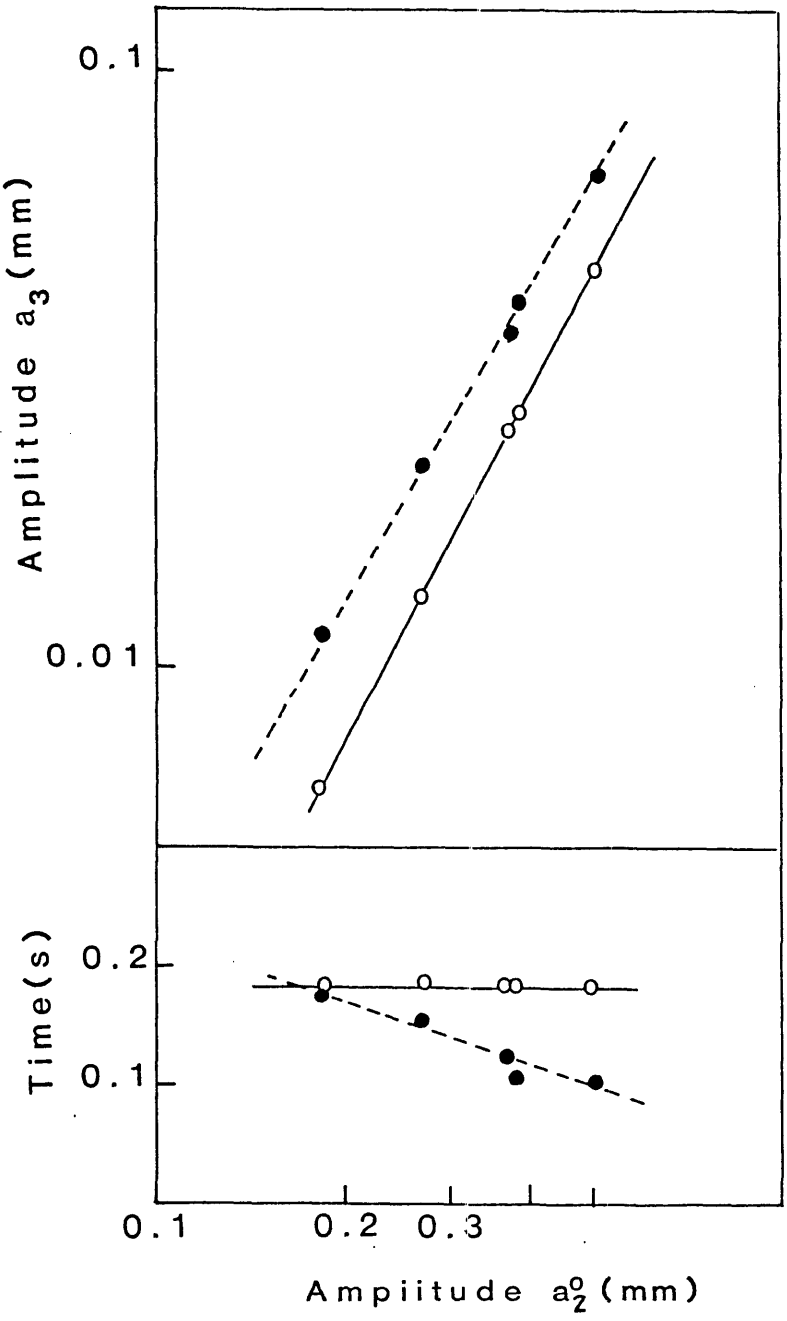

Figure 5.12: Calculated (open circles, full curve) and measured (filled circles, broken curve) dependance of the third mode peak amplitude a_3 and time delay on the initial amplitude a_2^0 of the second mode for a kinked bar struck at a node of the third mode.

The approximate agreement in slope and magnitude between the experimental and theoretical curves in Fig. 5.12 supports the general behaviour described by equation (5.45). The value of the parameter β_2 implied by the experimental results is about 4000 $m^{-1}s^{-1}$ which is rather larger than the theoretical value near 2560 $m^{-1}s^{-1}$ deduced from the physical dimensions of the bar, but the level of discrepancy is quite acceptable given the approximations in the theory and the uncertainty in the behaviour of τ_3 .

While it is quite obvious that further careful analysis and experimentation to determine the decay of the third mode as it is affected by amplitude and interactions with other modes may improve our results quantitatively it must be remembered that the object of our exercise was to identify the major physical mechanisms responsible for mode coupling. The reasonable agreement between theory and experiment that we have shown gives us confidence that we have indeed succeeded in our identifications. We have chosen therefore to press on and follow up the rather tempting speculation that similar mechanisms may be largely responsible for the transfer cascades observed in large-amplitude vibration of symmetrically flanged gongs.

More generally, we should expect mode coupling and energy transfer of this type to occur in all plate-like systems having a sharp kink or crease. Whether or not a significant amount of energy is transferred to the higher mode will depend upon the extent to which there is agreement between the frequency of a higher mode and that of the second harmonic of some other mode being driven to a large amplitude.

GLOSSARY OF SYMBOLS COMMONLY USED IN CHAPTERS 6 AND 7 FOR THE GONG.

r	radial position
θ	angular position
t	time
$u(r,t)$	circumferential component of displacement
$w(r,t)$	normal component of displacement
$x(t)$	temporal component of $w(r,t)$
a	amplitude of motion
b	motion centre
ω	radial frequency
ω_0	small-amplitude frequency of fundamental mode
ω'	forcing frequency relative to ω_0
m	effective mass
c	rigidity factor
k	damping parameter
x_0	height of dome
h	thickness
ρ	density
R	radius of curvature
F	stress function
E	Young's modulus
A	second-order nonlinearity parameter
B	third-order nonlinearity parameter
G	force per effective mass

Chapter 6

Review of the gong.

We have already stated in our "motivation" our belief that the "shimmer" of a gong is due to high frequency modes of vibration excited by nonlinear couplings to modes of lower frequencies. While there is very little work published on the acoustics of the gong, what there is does at least attempt to deal with nonlinear behaviour. Most related to the problem at hand, is a semi-quantitative investigation into the acoustics of a Tam-Tam (Rossing and Fletcher 1983(a)). The analysis included in this investigation, however, does little more than outline the form of the nonlinear equation of motion, a generalised version of the equations we have already encountered in Chapters 3 and 5 for the nonlinear string and bar respectively. Furthermore they propose that a number of hammered bumps situated in concentric rings around the gong's centre may play an important role in the transformation of energy between axisymmetric and asymmetric modes. Indeed they may, but the gong we are to investigate does not have such bumps and yet still displays mode coupling, albeit not quite so magnificently!

Perhaps more helpful to our particular investigations are two published works (Rossing and Fletcher 1983(b) and Fletcher 1985) which present qualitative and quantitative accounts respectively for the frequency shifts heard in certain types of gongs. Although the analysis here is really concerned with frequency shifts, we shall find that this is quite an important phenomenon occurring for our gong and may have a significant role to play in the exchange of energy between harmonically related modes. It is therefore worth our while to consider the quantitative analysis (Fletcher 1985) in the hope that it may throw a bit of light on a part of our problem. Fig.6.1 shows the profile of the gong analysed, which is similar to ours. Fletcher sidesteps the rigorous analyses of domes (we shall touch on these later)

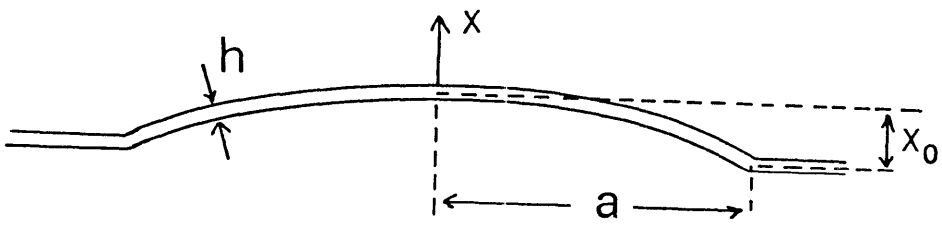

Figure 6.1: Profile of the gong analysed by Fletcher (1985).

and presents a rather elegant and simple analysis based on the actual mode shape of the fundamental symmetric mode. By considering the pattern to have no nodal lines or circles within the boundary, (a point we shall also contend with later) he derives an equation of motion for this fundamental mode

$$\ddot{x} + \omega_0^2 x = -\left(\frac{\omega_0^2 - \frac{c}{m}}{2x_0^2}\right)\left(x^3 + 3x_0x^2\right) - 2k\dot{x} \tag{6.1}$$

where ω_0 is the small-amplitude frequency limit, m is the effective mass and c is a rigidity factor. He then assumes a solution of the form

$$x = a\cos(\omega_0 t + \phi) + b \tag{6.2}$$

and solves (6.1) using the method of slowly varying parameters to find the variation of a and ϕ with time. While the results of this analysis show a frequency shift with amplitude they also suggest that the amplitude itself simply decays exponentially in time. Fletcher does, however, suggest a refinement of the approximation based on the fact that, physically, the form of x should really be written as

$$x = b + a_1\cos(\omega_0 t + \phi) + a_2\cos(2\omega_0 t + \phi) + a_3\cos(3\omega_0 t + \phi) \tag{6.3}$$

as suggested by the right-hand side of (6.1). Quite obviously we now have harmonics of the fundamenal mode but with the same spatial pattern. a_2 and a_3 can then be generated nonlinearly from a_1 so that, for small amplitudes, which, considering the rigidity of the gong we shall be investigating is certainly true in our case, a_2 varies like a_1^2 and a_3 as a_1^3 .

Apart from the aforementioned articles however, there is a scarcity of quantitative information on the gong itself. Since our specimen is little more than a spherical shell surrounded by a conical flange, a review of shells is therefore in order.

Benchmark Papers in Acoustics Volume 8 (Kalnins and Dym 1976) contains an illuminating introduction to its chapter on shells with a historical synopsis on the important papers published so far in the field. As our interest lies in spherical shells and in particular in the transverse vibrations of shallow spherical shells, we shall not dwell too much on the more general aspects.

Much of the foundation work done on spherical shells appears to have been done by Reissner. In particular (Reissner 1945) he derives a system of equations to describe the static deformation of thin shallow shells, where shallow refers to a ratio of height x_0 to base diameter r of less than $\frac{1}{8}$.

$$\nabla^2 \nabla^2 F - \frac{hE}{R} \nabla^2 w = -(1-u) \nabla^2 \Omega \tag{6.4}$$

and

$$D \nabla^2 \nabla^2 w + \frac{1}{R} \nabla^2 F = p - \frac{2\Omega}{R} \tag{6.5}$$

where F is a stress function, u and w are circumferential and normal components of the displacement respectively, E is Young's Modulus, h is the thickness of the shell, D is a rigidity factor equal to $\frac{Eh^3}{12(1-\nu^2)}$, ν is poissons ratio, R is the radius of curvature, p is an external load potential and Ω is the load potential such that $\nabla\Omega = p$. After an early attempt (Reissner 1946) at modifying the equations for the dynamic case and solving them by an approximate method, Reissner later realised (Reissner 1955) that for vibrations that are predominantly transverse, longitudinal inertia terms may be neglected in comparison to the transverse inertia terms. This then greatly simplifies the dynamic equations so that he finds

$$\nabla^2 \nabla^2 F - \frac{hE}{R} \nabla^2 w = 0 \tag{6.6}$$

and

$$D \nabla^2 \nabla^2 w + \frac{1}{R} \nabla^2 F = -\rho h \frac{\partial^2 w}{\partial t^2} + p(r, \theta, t) \tag{6.7}$$

which, after separation of variables, gives the spatial solution $w(r)$ for displacement as a sum of Bessel and modified Bessel functions,

$$w(r) = C_1 J_0(\lambda r) + C_2 Y_0(\lambda r) + C_3 I_0(\lambda r) + C_4 K_0((\lambda r) + C_5 \tag{6.8}$$

where

$$\lambda^4 = \frac{\rho h}{D} \omega^2 - \frac{hE}{R^2 D} \quad . \tag{6.9}$$

Establishing boundary conditions then enables determination of the constants and a relationship for the frequency of the modes. For example, for the clamped shell Reissner obtains

$$\omega = \left(\frac{E}{\rho}\right)^{\frac{1}{2}} \frac{h}{a^2}\left[\frac{\mu^4 + \kappa^4 \frac{1-\nu}{1+\nu}}{12(1-\nu)}\right]^{\frac{1}{2}} \tag{6.10}$$

where $\mu = \lambda a$ and $\kappa^4 = 48(1+\nu)^2 \frac{x_0^2}{h^2}$ which corresponds to the frequency of a flat plate when $\kappa = \nu = 0$,

$$\omega = \left(\frac{E}{\rho}\right)^{\frac{1}{2}} \frac{h}{a^2}\left(\frac{\mu_0^4}{12}\right)^{\frac{1}{2}} \quad . \tag{6.11}$$

The computation involved in obtaining the individual frequencies for the axisymmetric modes is obviously rather involved and Reissner only does it for the lowest mode of a clamped and a free shell in order to compare them with his earlier approximate results.

Equations (6.4) and (6.5) are again used (Johnson and Reissner 1958) to investigate, this time, the nonsymmetric transverse vibrations of a shallow spherical shell.

Hoppman (1961) refers to Reissners early attempt at solving the dynamic equations for symmetric vibrations and solves them himself by a more exact method. His work is of particular interest, not so much for the brief analysis, but rather that he includes numerical examples in his results. Unfortunately the ratio of physical dimensions he uses in his examples does not correspond even approximately to that of our gong and can therefore throw little light on our situation.

Kalnins (1961) analyses the complete spectrum of frequencies for spherical shells, deducing that it can be divided into three parts corresponding to the three dominant modes of vibration: thickness-shear, longitudinal and transverse. While he goes far beyond what is necessary for our uses, it is interesting to note that, although he determines that for nonsymmetric vibrations none of the three modes can exist uncoupled, he does confirm Reissner's earlier assumption that providing the frequencies of vibration are of the order of $\left(\frac{E}{\rho}\right)^{\frac{1}{2}} \frac{h}{a^2}$,then the vibrations are predominantly transverse and the other inertia terms may indeed be neglected.

Up till here all investigations appear to have been theoretical. We have the equations of motion for transverse vibrations of spherical shells, simplified so as to be solvable for shallow shells and solved for particular boundary conditions and physical parameters to give mode frequencies. Hoppman and Baronet (1963) saw the need at this point to dispel doubts as to the applicability of these results and so present an experimental investigation

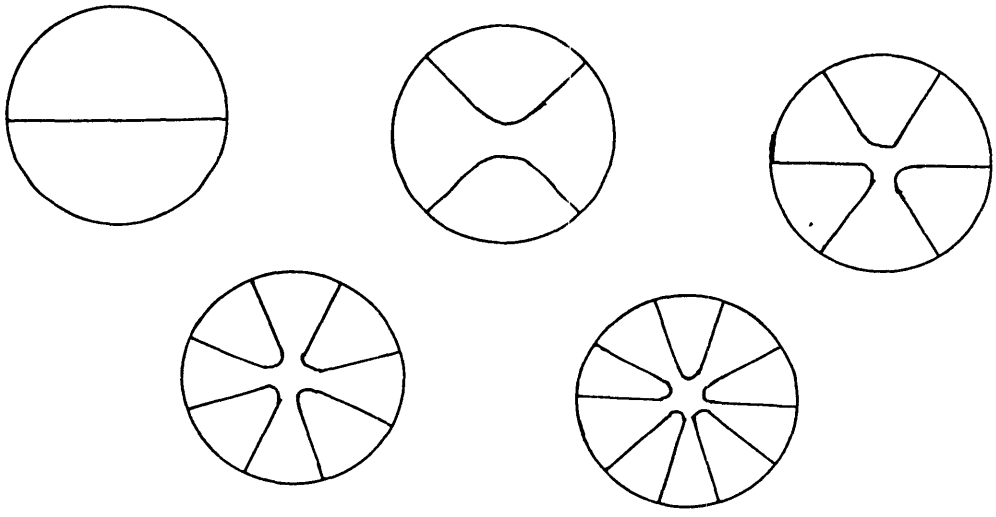

Figure 6.2: Nonaxisymmetric mode shapes of clamped and hinged shallow spherical domes as measured by Hoppmann and Baronet (1963).

into the mode shapes and frequencies for both symmetric and asymmetric vibrations of isotropic shells with either clamped or momentless (hinged) boundary conditions. Their experimental arrangement involved steel shells vibrated by means of an electromagnetic oscillator at the apex. The results of this experimentation are particularly interesting for a few reasons. Firstly they show reasonable agreement between theory and experiment. Secondly, the asymmetric mode shapes shown have nodal lines that do not cross in the centre but look like solutions for a system whereby the radial and angular components are not separable (Fig.6.2), although theory obviously states their separability. This somewhat surprising result is most likely caused by the fact that the oscillator was situated at the centre of the shell thereby forcing that point to vibrate and thus the mode shapes to become a combination of symmetric and asymmetric modes. This phenomenon will be dealt with in a little more detail in chapter 7 when we come to examine the mode shapes of the gong. Finally the authors point out that the fundamental symmetric vibration has two nodal circles, one at the boundary and the other closer to the centre. As the height of the dome is decreased, the latter circle approaches the boundary until, in the limiting case of a flat plate, the two circles are coincidental on the boundary. This then suggests that Fletcher's analysis for the frequency shifts of the gong (Fletcher 1985) may not be strictly correct as

he approximates his gong to be a rigidly clamped dome and assumes a mode shape for the fundamental with no nodal lines or circles within the boundary.

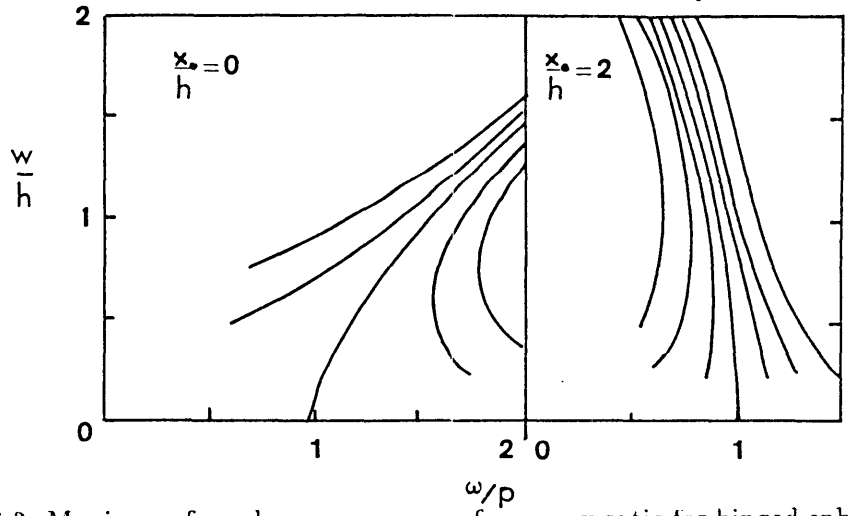

Figure 6.3: Maximum forced response versus frequency ratio for hinged spherical caps (from Grossman, Koplik and Yu 1969).

Thus with the establishment of the free transverse vibrational modes of a shallow spherical shell, we turn to nonlinear investigations on them. Grossman, Koplik, and Yu (1969) investigate the effects of curvature on the axisymmetric vibrations of spherical shells with various edge conditions. The effects of curvature are introduced into the equations for displacement and strain and, as with most nonlinear equations a series of approximations must be made to solve the resulting equations of motion. The exact analysis need not concern us here as again there is a dependency on boundary conditions and physical parameters that do not fit our gong but the results are interesting if we consider the trends they depict. Fig. 6.3 shows the response curves for a shell with hinged edge conditions for the curvatures $\frac{x_0}{h} = 0$ and $\frac{x_0}{h} = 2$. There is obviously a transition from a hardening to a softening type of nonlinearity. Fig. 6.4 shows how the linear fundamental frequency for a particular shell changes with curvature. Note the obvious dependence on boundary conditions.

All this brings us back to our own case. We have a shallow spherical dome and thus may expect behaviour, both linear and nonlinear as described above but we have most unusual boundary conditions, a conical flange. While we may therefore take this review as a basis for our investigations, the obvious reliance of the exact behaviour of a spherical shell on boundary conditions must warn us that we are, together with Fletcher and Rossing, attempting to solve the nonlinear where the linear is not yet fully established.

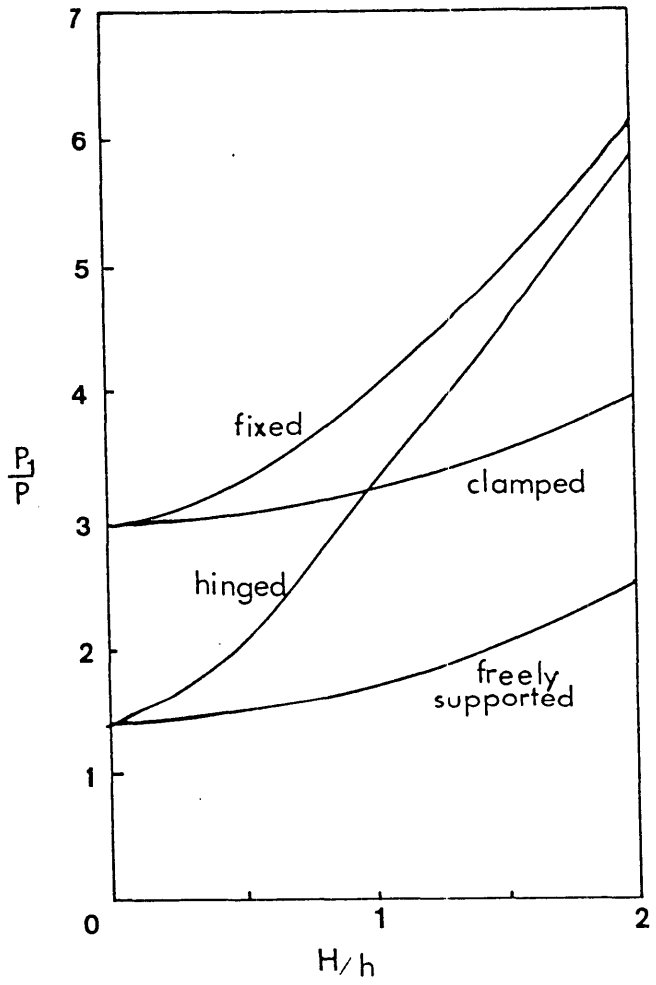

Figure 6.4: Linear fundamental frequency versus rise for fixed, clamped, hinged and freely supported spherical caps (from Grossman, Koplik and Yu 1969).

Chapter 7

The gong.

One only has to consider the linear analysis of the transverse motion of shallow spherical shells (Reissner 1955) to realise that an attempt at a rigorous and quantitative analysis of mode coupling on the gong would not be realistically possible at this late stage. Indeed one would have to devote ones entire thesis alone to do an adequate job on it. We shall therefore reverse the trend followed in chapters 3 and 5 of analysing the situation theoretically and performing experiments to confirm the predictions made. In this chapter we shall use the generalised predictions made in chapter 5, namely that mode coupling and energy transfer should occur in all plate-like systems having a sharp kink or crease as we found it happened for the kinked bar. We shall attempt to show experimentally that this does indeed happen. We shall see that the system is highly complicated and may even require an analysis involving bifurcation and chaos theory for a multimode system, indeed a thesis in its own right!

7.1 Description of the gong used.

The gong we used in our experiments (Fig.7.1 & Fig. 7.2) was made by the Zildjian company from a 2mm thick bronze alloy. The central domed section of the gong had a base diameter of 50cm and a dome height of 5mm. It was quite obviously well within Reissner's definition of a shallow dome whereby the ratio of the dome height to the base diameter should be less than 1/8.

The dome was surrounded by a 5cm conical flange. In the very centre of the gong was a 1.25cm diameter hole via which some sort of lathe may have held the gong during its

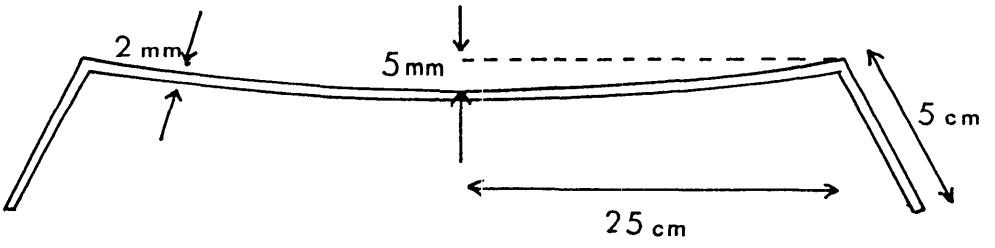

Figure 7.2: Cross-section of gong showing dimensions.

making. Over the entire surface, dome and flange, there was a series of concentric rings, centred on the centre of the gong seemingly pressed into the metal as it spun in the lathe. These rings will tend to increase the stiffness of the gong for the nonaxisymmetric modes and hence raise their frequencies whilst having little or no effect on the axisymmetric modes.

The gong appears to have been made by a method quite different from the ancient craft of hammering a gong into shape by hand. In fact it seems to have had a making more akin to that of a cymbal for which, of course, Zildjians are most famous. Whatever its origin, the sound of our gong displays the same type of nonlinearity as a traditional chinese tam-tam although, to the ear, not quite as obviously. Its more simple physical characteristics however, may also prove an advantage in any attempt we make to compare theoretical analysis with experiment.

7.2 Preliminary experiments.

Quite obviously the first step before we even consider nonlinearity is to aquaint ourselves with the normal modes of vibration of our gong. This was done by vibrating the gong with white noise via a pin through its centre, using a Bruel & Kjaer shaker (type 4810) and measuring the admittance with an impedance head (type 8001) and an HP 2-channel FFT analyzer (type 3582A). While this may cause us to be looking only at the axisymmetric modes it is appropriate considering that in normal practice the gong is struck at its centre, suggesting that the axisymmetric modes are the first to be initiated.

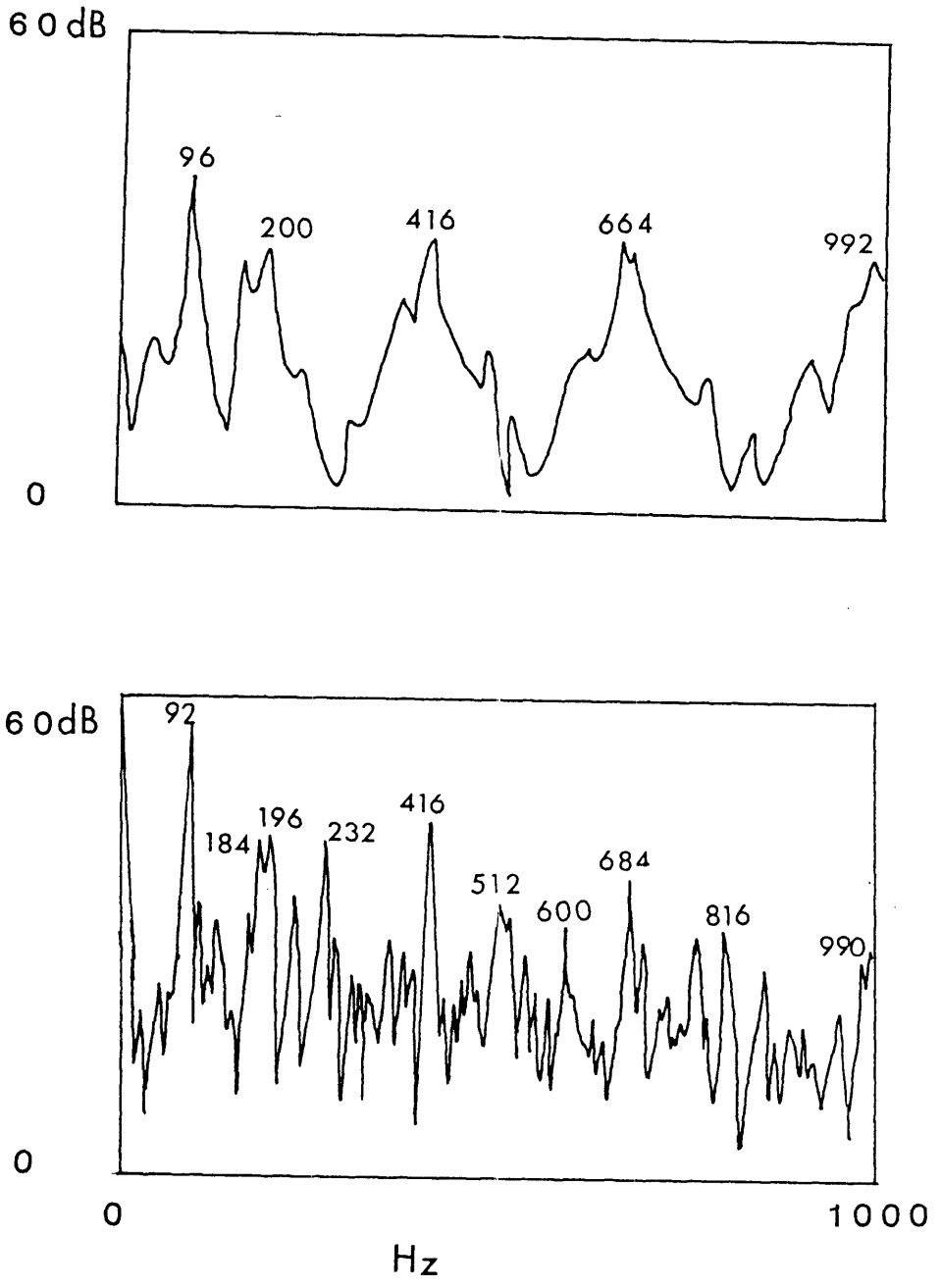

Figure 7.3: (a)Admittance spectrum of the gong when shaken via a pin through its centre.(b) Velocity spectrum of the struck gong.

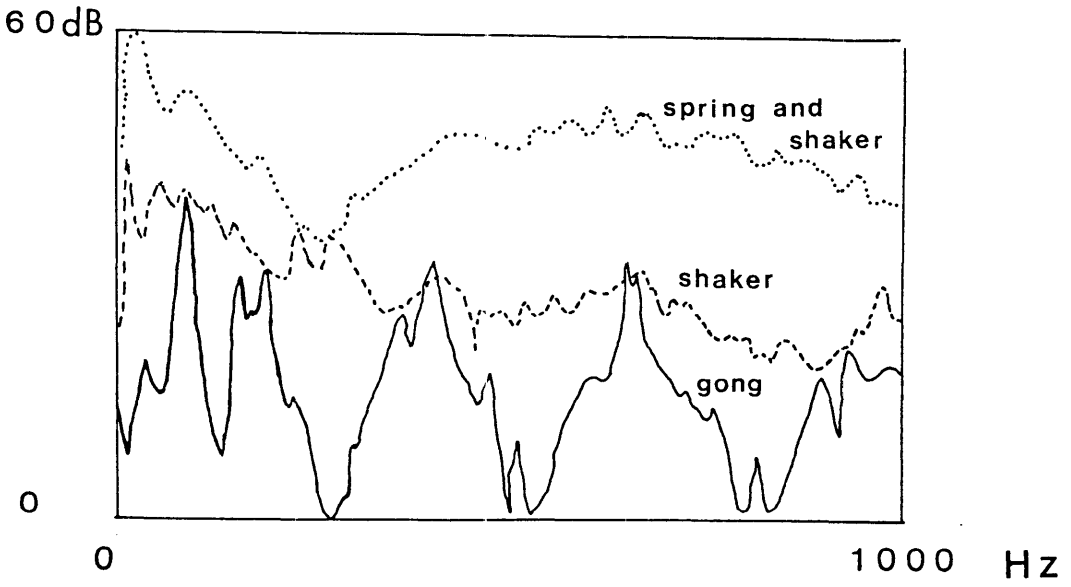

Figure 7.4: Admittance spectra for (i) the shaken gong ,(ii) the shaker and (iii) the shaker and a short stiff spring.

The results are shown in Fig.7.3 for the frequency range of 0-1 KHz together with a typical initial velocity spectrum for a struck gong. Presuming the amplitude of vibration was sufficiently small in the case of the shaken gong so that no significant nonlinearities came in to play, then we can see a trend suggesting that nearly integral relations between mode frequencies could be important for the sound of the gong.

It is, at this point, worth noting a measure taken to ensure that the shaker does not make the gong behave as though it has a mass fixed to its centre and hence affect results. Fig.7.4 shows the admittance of the shaker alone, measured by means of a second shaker, and superimposed on the previously measured admittance of the gong. While the admittance of the shaker can be seen to be generally higher than that of the gong, it is worthwhile, as a precautionary measure for later more intricate experiments, to insert a spring between the gong and shaker. The load on the gong therefore becomes springlike; Fig. 7.5 depicts the equivalent circuit.

A short and moderately stiff spring had one end firmly clamped while 100g weights were added to the other end and the extension of the spring was recorded for the addition of each weight. Fig 7.6 depicts the results as plotted as N vs m and shows the compliance of the spring to be approximately 2.0×10^{-4} Nm^{-1}. The spring obviosly obeys Hookes law within

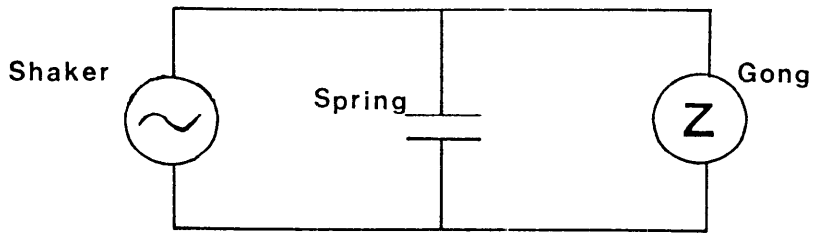

Figure 7.5: Equivalent circuit for a gong shaken by the shaker with a moderately stiff spring between gong and shaker.

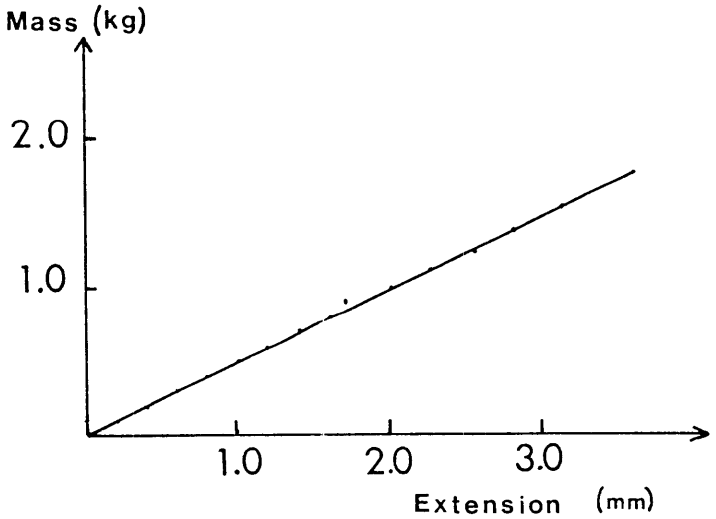

Figure 7.6: Compliance of the spring.

the amplitudes of vibration we shall be using. The combined admittance of the spring and shaker was compared again to the gong admittance (Fig. 7.4) and can be seen to be well higher.

Having established the normal axisymmetric mode frequencies it was then quite a simple matter to measure the individual modal patterns by shaking the gong, again via a pin through its centre, at particular frequencies and detecting the nodal lines with a Bruel & Kjaer subminiature accelerometer (type 8307). Fig.7.7 shows the first five symmetric modes corresponding to the first five resonance peaks in Fig.7.3. It is interesting to note the position of the nodal circle on the lowest mode. If the gong was behaving as a clamped spherical shell we would expect two nodal circles, one at the kink and another towards the centre (Hoppmann and Baronet 1963). Clearly this is not so, but rather it is behaving somewhat as Fletcher(1985) suggested although the nodal circle is not situated at the kink. By comparison all the other modes appear to have a nodal circle close to the kink. The fact that the gong is freely suspended rather than rigidly clamped means it will have some motion as a whole thus accounting for this shifting of the nodal circles .

A few asymmetric modes were also mapped for frequencies at which the gong resonated while the shaker was attached to the centre of the gong and they are depicted in Fig.7.8(a). They are similar in shape to the modes depicted by Hoppmann and Baronet (1963).Fig.6.2.for their clamped spherical shell. These shapes appear to be a mixture of axisymmetric and asymmetric modes suggesting that the angular and radial components of the motion are not separable unlike theory suggests (eg. Reissner 1955). Considering, however, that in both experimental arrangements, the shell was shaken at its centre it is not really all that surprising that the nodal lines fail to cross there. The asymetric modes can still be excited if they are not exactly antisymmetric. A quick experimental check was performed by vibrating the gong off centre at the appropriate frequncies. The results show a better separation of radial and angular components (Fig.7.8(b)).

7.3 Frequency shifts with amplitude.

We encountered in chapter 6, predictions of a frequency shift with amplitude in the fundamental mode of vibration. Fletcher(1985) showed that the fundamental frequency for a spherical dome should decrease quite sharply with increasing amplitude until the amplitude was approximately $0.8x_0$ whereupon it would rise for even larger amplitudes. In our case,

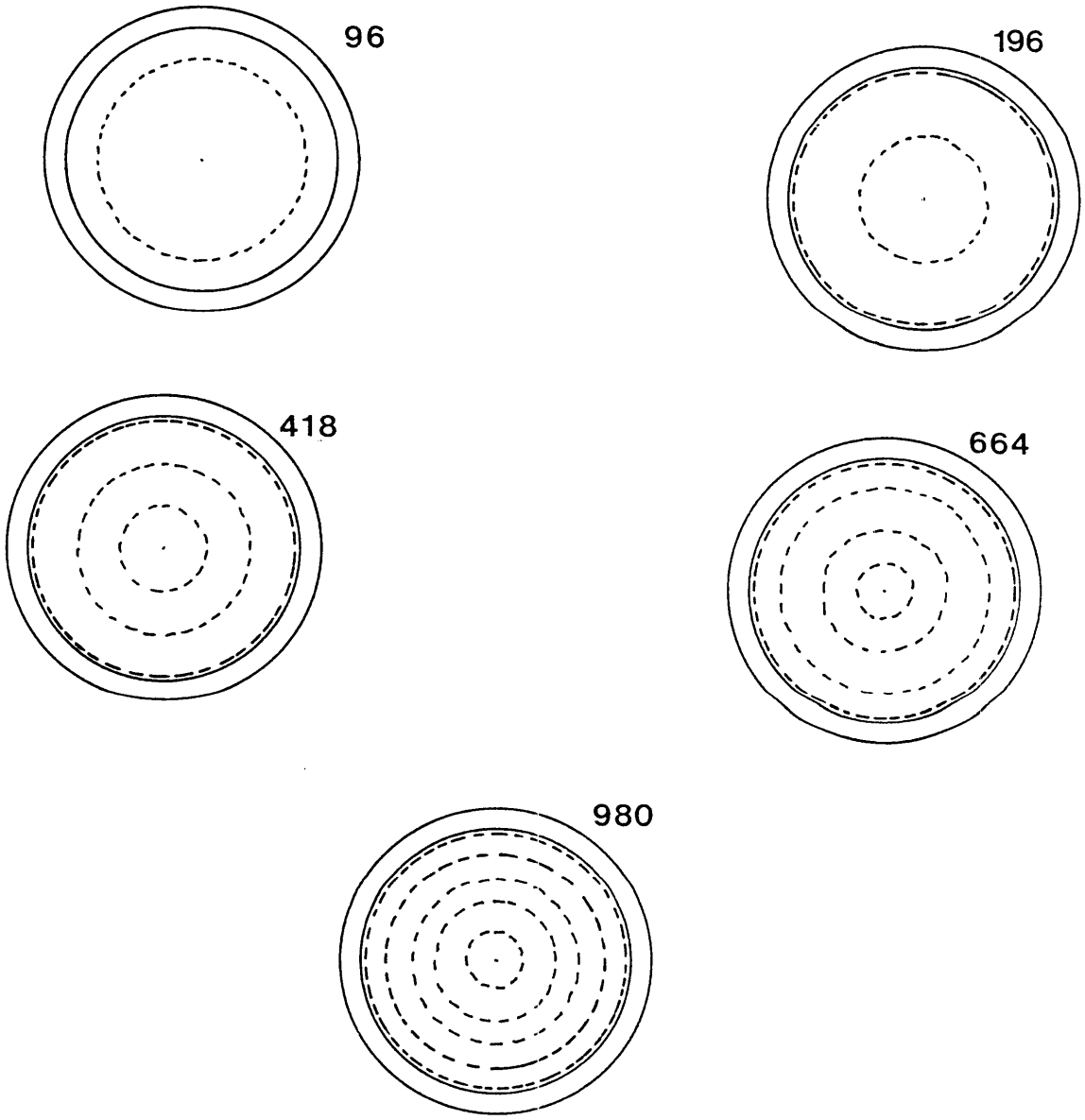

Figure 7.7: Measured modal patterns for the first five axisymmetric modes of our gong.

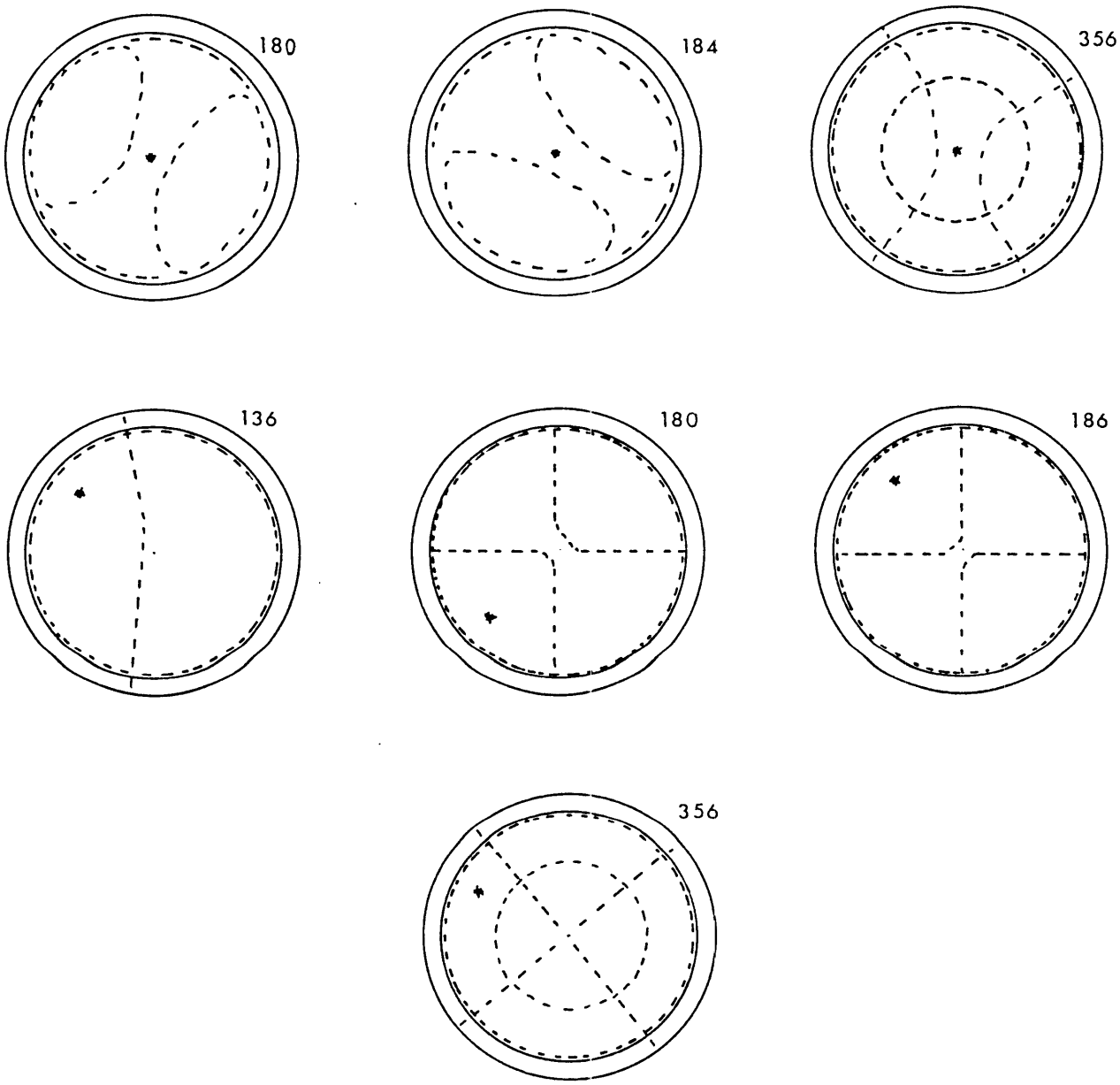

Figure 7.8: Measured asymmetric modal patterns for our gong when shaken (a) at the centre and (b) at a position marked with an asterisk.

with a dome height of 5mm and an extreme amplitude of motion of no more than that, we expect to see nonlinear frequency shifts of the softening type.

The frequency shift of the fundamental mode for a moderate strike was roughly measured as follows: The Bruel & Kjaer subminiature accelerometer was attached near the centre of the gong and the signal generated by striking the gong was fed, via an amplifier, into a Nagra IV tape recorder. The signal could then be analysed repeatedly on a Hewlett Packard Spectrum Analyser (type 3582A). By triggering the spectrum analyser externally with a variable delay trigger pulse, the velocity spectrum was obtained for 0.5 sec time intervals. The results in the following table show that the fundamental varies in frequency from 90 Hz initially, corresponding to a fundamental amplitude of about 1.4mm, to 96 Hz in the small-amplitude regime for amplitudes of less than 0.63mm.

Amplitude(mm)	*Frequency(Hz)*$\pm$2	*Time(s)*
1.4	90	0
1.2	92	0.5
1.1	94	1.0
0.92	94	1.5
0.77	94	2.0
0.63	96	2.5
0.6	96	3.0
0.48	96	3.5

A quick graphical comparison of these results with those predicted by Fletcher (1985) shows reasonable agreement in how the frequency of the fundamental mode changes with amplitude (Fig.7.9).

The frequencies of the higher modes were also seen to change with time and therefore one suspects, with amplitude, however the complexity of the system is too great for any meaningful results to be extracted. The growth of resonance peaks at harmonics of the fundamental appears to suggest mode coupling but the initial presence of modes close to those frequencies makes further investigations by this method impossible.

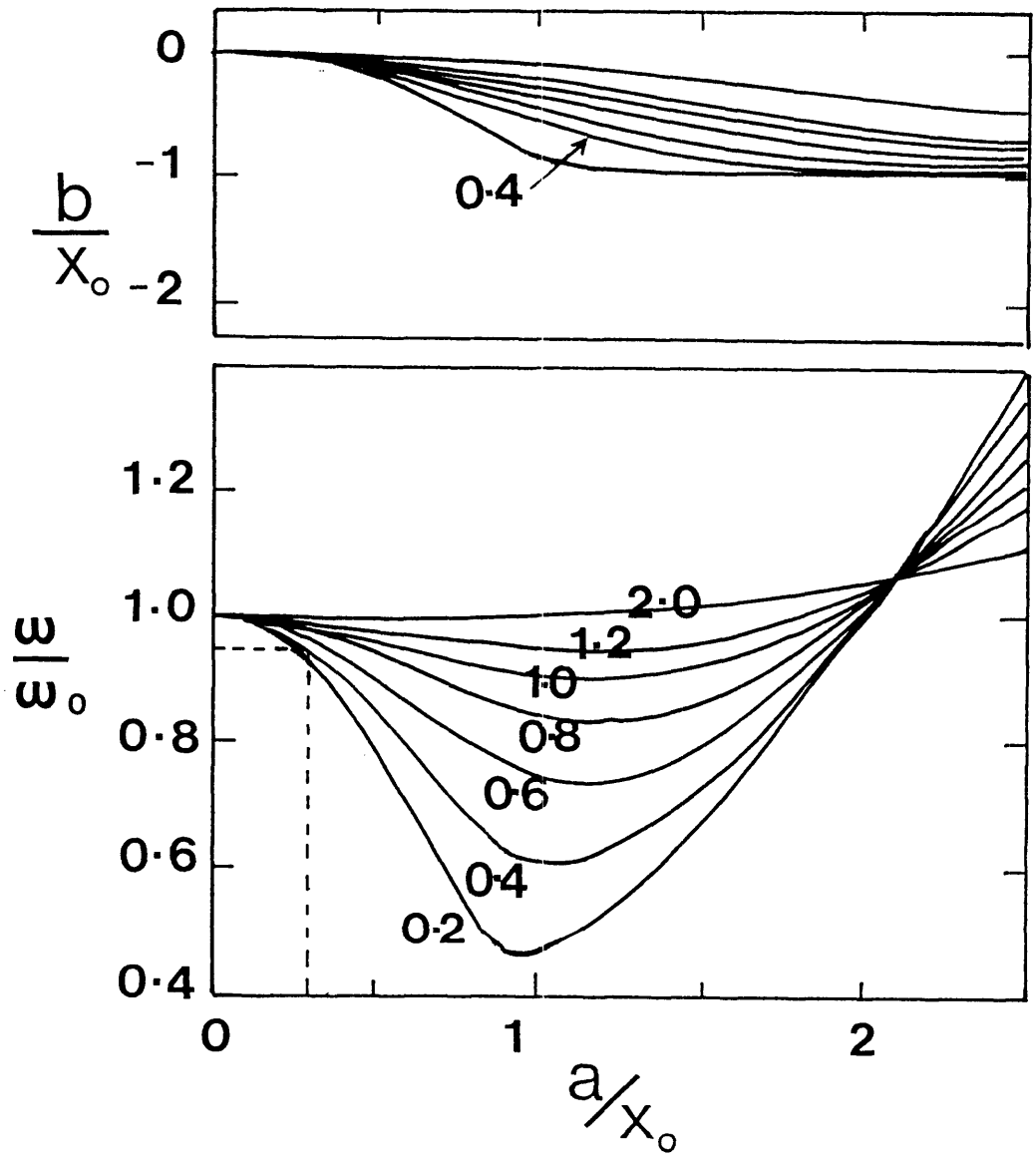

Figure 7.9: Calculated motion centre b and frequency ω for vibrations of amplitude a on a spherical shell of dome height x_0 when the normalised shell thickness $\frac{h}{x_0}$ has the value shown as a parameter (from Fletcher 1985). For our gong $\frac{h}{x_0} \approx 0.4$. The dashed line depicts the amplitude 1.4mm.

7.4 Preliminary investigations into mode coupling.

Bearing in mind that we have so far, only our generalised results for the kinked bar to base a hypothesis on, we begin our mode coupling investigations with an experiment similar to that performed on the bar. Our hypothesis is that the gong, being essentially a spherical shell with a kink around it, should display second and third order nonlinearities such that the amplitude of the second and third harmonic modes of a particular frequency should vary with the fundamental amplitude, a_1 ,like a_1^2 and a_1^3 respectively. Furthermore, if these higher modes are generated to large enough amplitudes, they in turn, could then generate their own harmonic modes by similar methods. This means that, for a particular fundamental frequency of amplitude a_1, we might expect to see a_2 varying as a_1^2 and a_4 varying as a_2^2 and therefore a_1^4 and so forth.

With the shaker again attached to a pin through the centre of the gong and a spring, as mentioned earlier, between the gong and the shaker to avoid a mass loading on the gong, the system was set to vibrate at the small-amplitude fundamental frequency of the gong, 96 Hz. The accelerometer was attached to the gong at a point on the nodal circle of this mode thus ensuring that measurements of the amplitudes of harmonic modes were actually higher modes of vibration and did not have the same spatial pattern as the fundamental mode (Fletcher 1985). The output of the accelerometer was then displayed, via an amplifier and appropriate filter. The amplitudes of the first three higher harmonic modes were measured as a function of the fundamental amplitude at the centre of the gong. Fig.7.10. depicts the amplitudes a_2 , a_3 and a_4 of the second, third and fourth harmonics respectively, each as a function of the fundamental amplitude a_1 , on log-log axes. The slopes of the resulting straight lines are 2.0 ± 0.2, 3.0 ± 0.3 and 4.1 ± 0.3 respectively. Clearly the trends agree with our hypothesis, that is, the amplitudes of the second, third and fourth harmonics vary as a_1^2 ,a_1^3 and a_1^4 respectively. Furthermore, although a_2 is present with relatively small fundamental amplitudes, a_3 and a_4 are negligible until a_1 has reached 0.3mm, in line with their being higher order nonlinearities and therefore requiring larger fundamental amplitudes to be generated significantly.

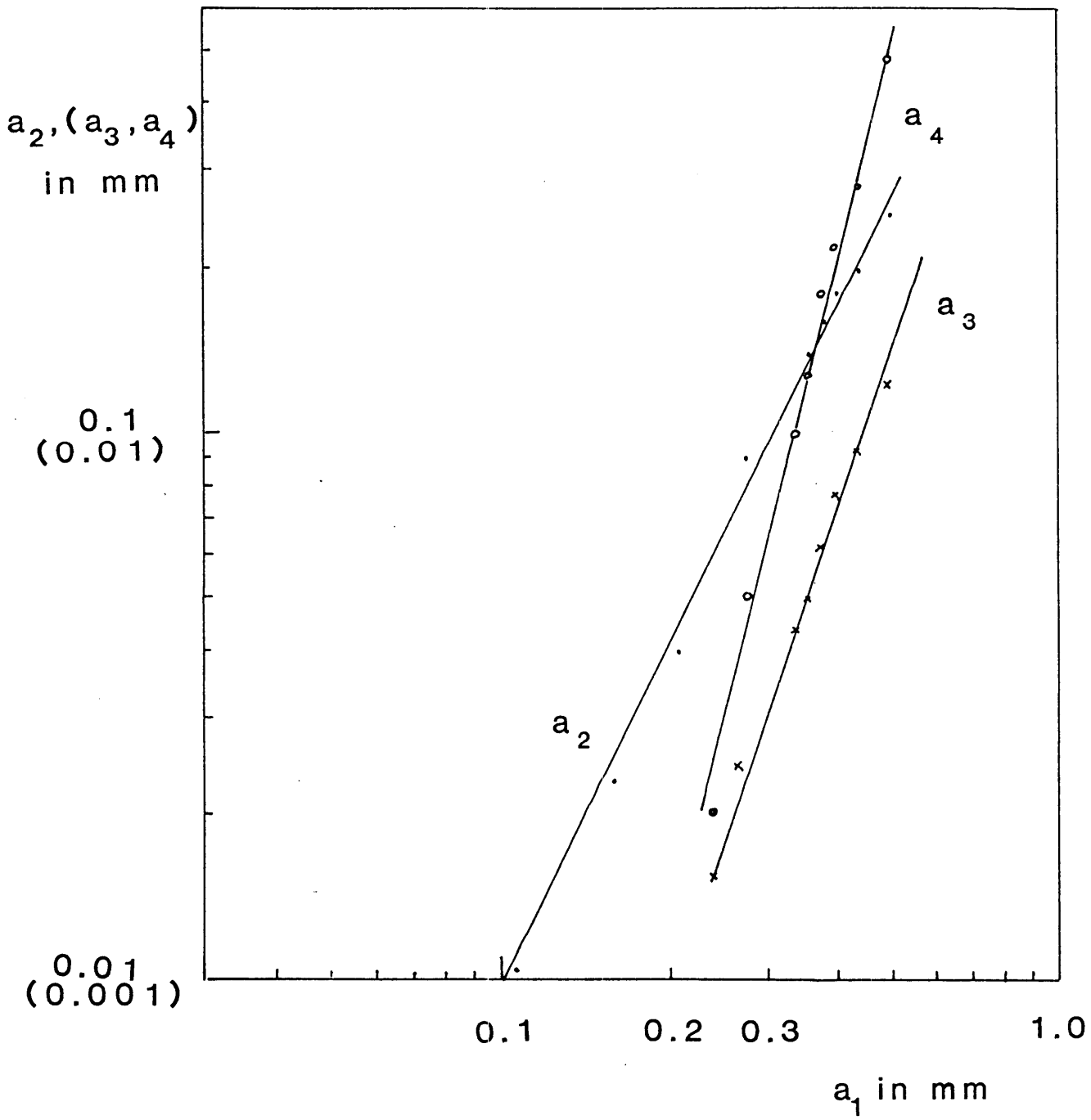

Figure 7.10: Amplitudes of the first three harmonics of the fundamental as they vary with the fundamental amplitude.

7.5 Random behaviour.

The investigation mentioned above into our cascade hypothesis, while unexciting in itself, produced an unexpected and interesting phenomenon. At particular frequencies and amplitudes the gong began to resonate at, what was obviously to the ear, more than just the fundamental frequency with a few overtones. Subharmonics could be heard clearly and, for some frequencies, the sound built up to the polyphonic "shimmer" of a struck gong.

Fig.7.11 compares the frequency spectrum of the gong's velocity with the frequency spectrum of the forcing term. This latter spectrum enables us to ensure that there was no significant coupling between the motion of the gong and the motion of the shaker such as to cause the forcing term to be nonlinear. We see from Fig. 7.11 that a force of amplitude 7.8N and frequency 91 Hz causes the period of the gong to bifurcate so that 45 Hz is generated whereas for a periodic force with amplitude of only 6.5 N and frequency 181 Hz the resulting motion of the gong is polyphonic.

By placing a Bruel & Kjaer Capacitive Transducer (type MM 0004) a short distance from the accelerometer already on the gong, the displacement of that point could be observed as a function of velocity. We can see in Fig.7.12(a) the bifurcation of state space into two for the forcing frequency of 91 Hz. For the more complicated case when the gong was forced at 181 Hz, the orbit was recorded at a set point once per cycle by use of the intensity modulator on the storage oscilloscope thus displaying Poincare points. Fig.7.12(b) shows that the motion is clearly more than simple bifurcations although the attractor obtained is rather featureless compared to calculated attractors. We need to consider two aspects of the situation however that may account for this. Firstly the large number of degrees of freedom may make the attractor very complex and secondly the experimental set-up allowed motion of the gong as a whole and this may have blurred the detail of the attractor.

It became clear during the course of the measurements that the type of behaviour depended acutely on the frequency at which the the gong was being forced and that a change in frequency by just a fraction of a hertz could produce a very different result. Just how the behaviour changes with amplitude and frequency can be seen in Fig.7.13. It must be noted here that the size of the shaker available for our experimentation limited the magnitude of the force we could apply to the gong to less than 8 N. A further complicating factor arises from the fact that the final behaviour arrived at by the gong may take quite a number of seconds to evolve, depending on the exact frequency and amplitude of the

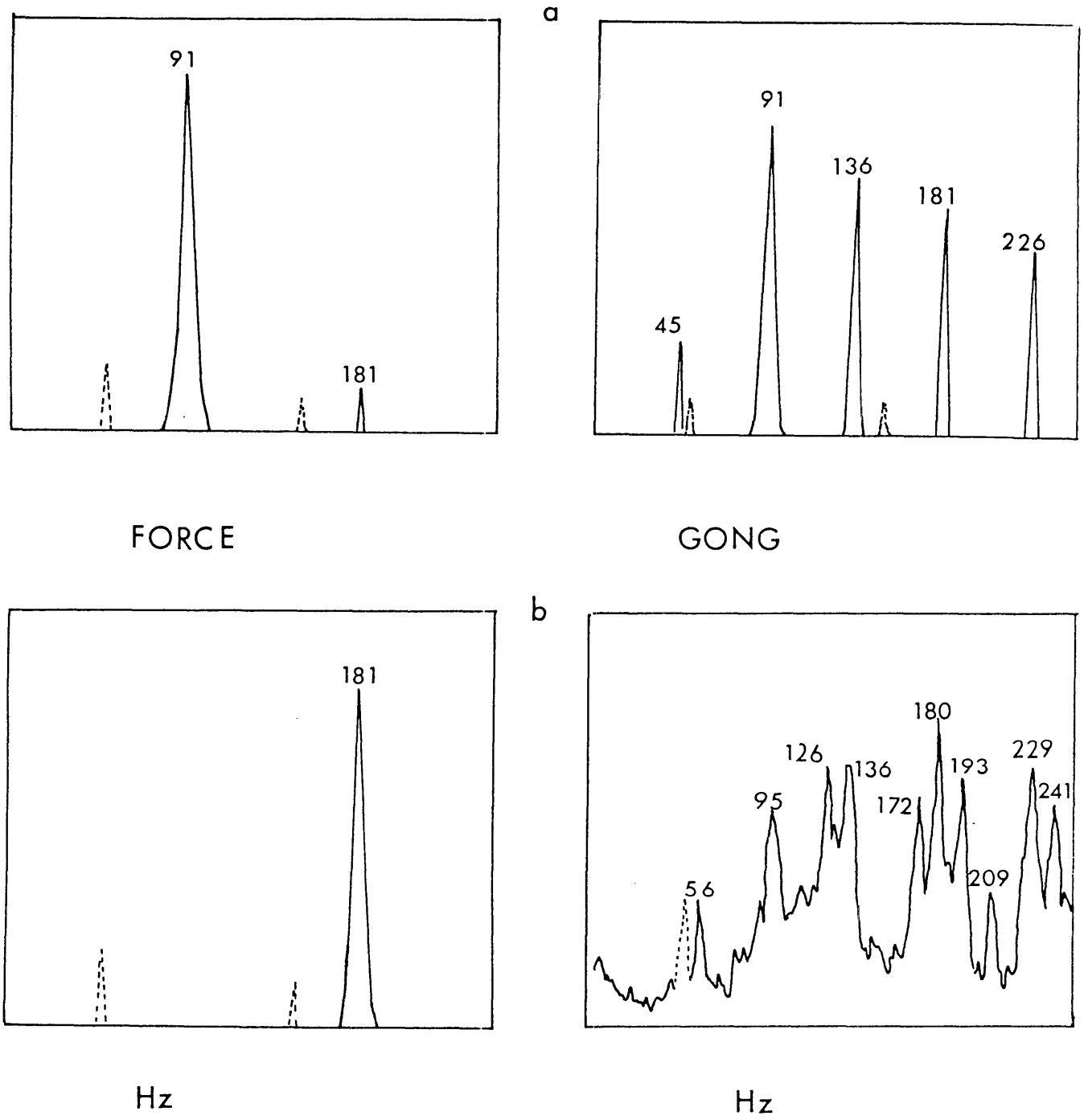

Figure 7.11: Velocity spectrum for the gong compared to that of the force (a) when the gong is forced at 91Hz and (b) when the gong is forced at 181Hz.

(a)

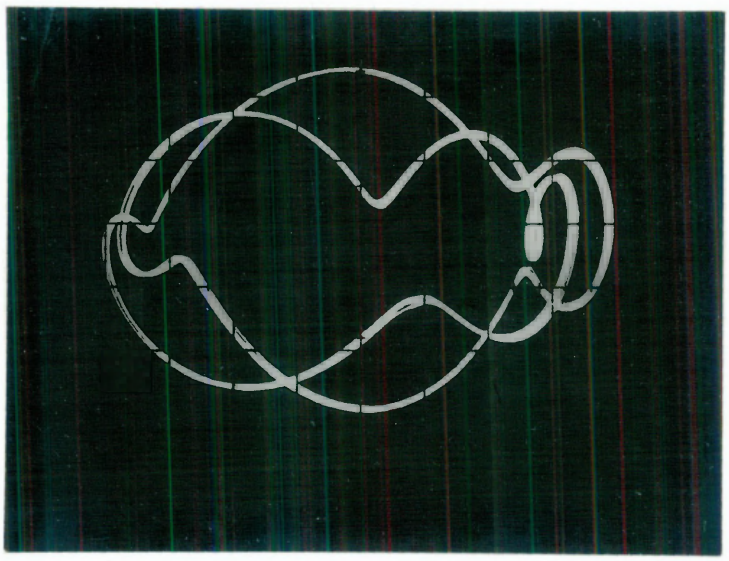

(b)

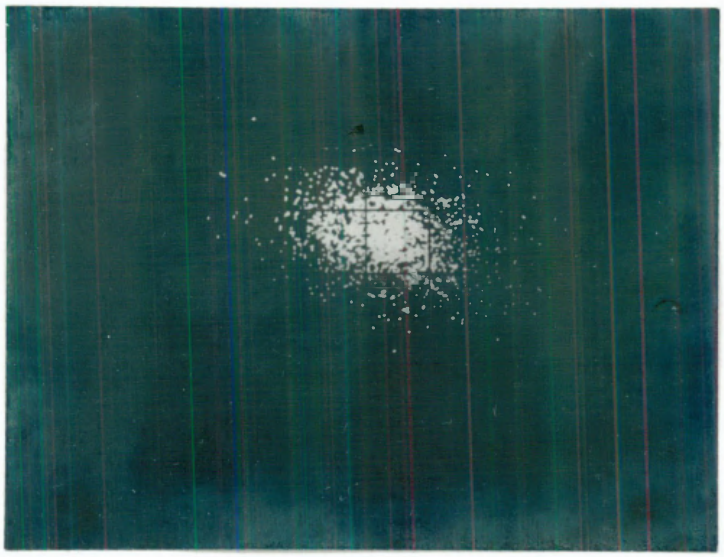

Figure 7.12: (a)Bifurcation of the state space orbit into two when the gong is vibrated at 91 Hz. (b) Strange attractor depicted by observing one point per orbit when the gong is vibrated at 181 Hz.

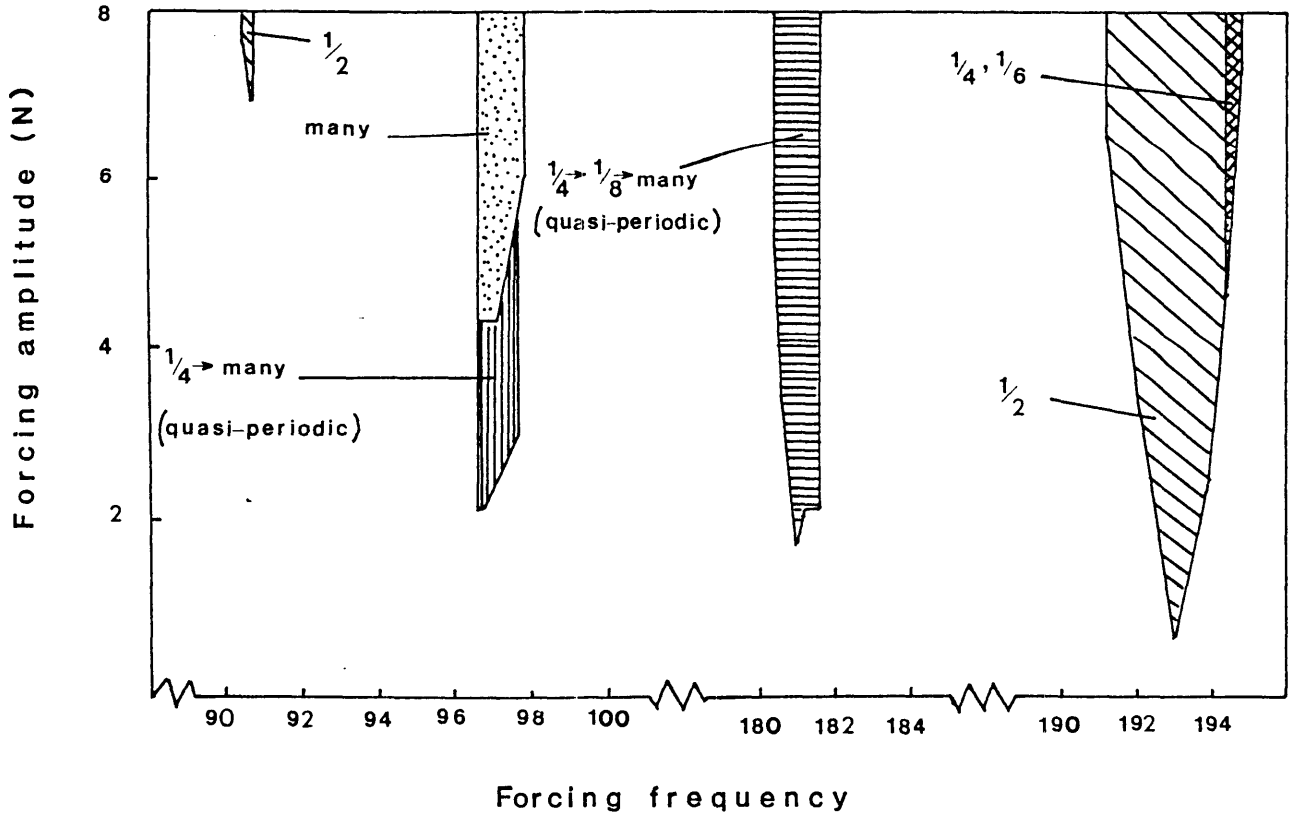

Figure 7.13: Response of the gong for varying frequencies and amplitudes of the force.

driving force. The Poincare points could be observed in such cases splitting from, say, 4 points to 8 points to many points for a particular steady forcing amplitude. Furthermore, the points occasionally became rings suggesting that the driven frequency was not quite a perfect subharmonic of the forcing frequency. The presence of such motion meant that the exact determination of the number of bifurcations occuring could become difficult. Fig. 7.13 is labelled "quasi-periodic" in areas of parameter combination where this difficulty could be incurred, and as such, the behaviour displayed in these areas must be taken as an estimation of what is happening.

While it must be remembered that we set out to investigate the struck gong as opposed to the periodically forced gong, the above phenomenon is actually more relevant than may at first be apparent. The fact that the sound at times appeared to be very similar to the sound of a struck gong after the higher modes have built up, suggests that we may have here a similar mechanism for mode conversion. It is worth our while therefore to look a bit more closely at the situation.

7.6 Chaos.

Had it not been for the investigations into strange attractors and chaos within the last decade, one might be forgiven at this point for describing the above phenomenon as a result of the complex behaviour of a multimode system and doing little more than tabulating a series of experimental results. Bearing in mind however, that chaotic motion is described as bounded oscillations with an infinite array of frequencies and, furthermore, that the road to chaos is along multiple bifurcations . we must recognize the above results as an exciting practical example of chaotic motion.

The complicating factor in our investigations will be that we are dealing with a multimode system and most of the literature on chaotic systems deals only with single mode systems. Nevertheless it is worthwhile pursuing a simple theoretical investigation into the motion to ascertain whether bifurcation and chaos may be causing the observed phenomena in both the shaken and the struck gong.

7.7 The gong as a single mode system.

Let us start by assuming the gong is just a single mode system where the mode is equivalent to the fundamental mode of a very shallow real gong, that is, it vibrates with no nodal lines or circles within the flange. Fletcher(1985) has shown the equation of motion for such a mode forced at a frequency ω' times the mode frequency by a force per unit effective mass, G, to be of the form

$$\ddot{x} + 2k\dot{x} + x + Ax^2 + Bx^3 = G\sin\omega' t \tag{7.1}$$

where k represents damping and A and B describe the nonlinearity associated with the gong. Note too, that the small-amplitude frequency of the gong has been normalised to unity.

If $A = 0$ then we have a generalised Duffing's equation. Particular examples of Duffing's equation have already been shown to exhibit chaos (Ueda 1979; Tongue 1986). Ueda investigates the particular equation

$$\ddot{x} + 2k\dot{x} + x^3 = G\cos t \tag{7.2}$$

for various values of k and G to show the dependence of the type of behaviour exhibited, on the system's parameters. Tongue investigates the existence of chaos in Duffing oscillators in an attempt to discover the reason why certain systems support chaotic motion.

As neither investigation covers the parameter values and combinations relevant to our gong, we must proceed with our own investigations to determine possible combinations of k and G for non-zero A that may support subharmonic bifurcations and chaotic motion.

We have seen that (7.1) may be written more particularly (Fletcher 1985) as

$$\ddot{x} + 2k\dot{x} + x + \left(\frac{1 - \frac{c}{m}}{2x_0^2}\right)(x^3 + 3x_0x^2) = G\sin\omega' t \tag{7.3}$$

where x_0 is the height of the dome, c is a rigidity coefficient due to the stiffness of the gong and m is the effective mass associated with the mode.

By comparing Reissner's (1946) approximate expression for the frequency of the lowest mode of a clamped shallow spherical shell, with his own expression for the small-amplitude frequency of the mode, Fletcher shows that

$$\frac{c}{m} \approx \left[1 + 0.85\left(\frac{x_0^2}{h^2}\right)\right]^{-1} \tag{7.4}$$

where h is the thickness of the gong.

We can, therefore, determine approximate values to within 20% for the second and third order nonlinear parameters A and B of equation (7.1). Hence, for our gong (in S.I. units), we obtain the expression

$$\ddot{x} + 2k\dot{x} + 253x^2 + 16840x^3 = G\sin\omega' t \tag{7.5}$$

7.8 Evaluation of parameters k and G.

Comparison of (7.5), the predicted behaviour for the fundamental mode of the gong, with the behaviour actually observed, obviously requires measurement of the damping parameter k as well as typical forcing amplitudes.

The measurement of k was quite simple. The gong was shaken at a particular frequency but with only a moderate amplitude to avoid too much nonlinearity, and the output from a subminiature accelerometer, situated on the back of the gong, was fed, via an appropriate filter to a storage oscilloscope. The time for the amplitude to decay by a factor of $\frac{1}{e}$ when the force ceased was then measured. The results for 3 different modes are displayed in the next table. The actual calculation of k had to take into account the normalising of the mode frequency to 1.

Frequency(Hz)	k
96	0.007
180	0.0007
196	0.002

Determination of the normalised forcing amplitude G was not quite so straight forward. Whilst measurement of the actual force in Newtons applied to the gong was quite simple, requiring only a calibration between the current flowing to the shaker and the force resulting from the current, it must be remembered that the parameter G in (7.5) is, in actual fact, the force per effective mass m of the mode. To calculate m we really need to consider the origins of the equation of motion (7.5) and to do this we must go back to Reissner's (1955) investigation into the axisymmetric modes of a shallow spherical shell.

We saw in chapter 6 that the form of Reissner's equation of motion is

$$\rho h\frac{\partial^2 w}{\partial t^2} + D\,\nabla^2\,\nabla^2 w = \Gamma \tag{7.6}$$

where we have written Γ as a function to include both the stress function of the gong and the applied force. The spatial solution of the homogeneous equation for the axisymmetric modes, taking into account the assumed boundary conditions of a clamped edge is, from (6.8), just

$$W(r,\phi) = \sum_n W_n(r,\phi) = \sum_r [C_{n1}J_0(\lambda_n r) + C_{n3}I_0(\lambda_n r) + C_{n5}] \tag{7.7}$$

where boundary conditions give

$$C_{n3} = C_{n1}\frac{J_1(\lambda a)}{I_1(\lambda a)} \tag{7.8}$$

and

$$C_5 = -C_1\left[J_1(\lambda a)\frac{I_0(\lambda a)}{I_1(\lambda a)} + J_0(\lambda a)\right] \quad . \tag{7.9}$$

To obtain an equation of motion for a particular mode p of the bar we must follow a similar procedure used in the earlier investigations of the string and the bar, that is, we multiply equation (7.6) by a particular spatial solution $W_p(r,\phi)$ and integrate over the surface of the gong.

The entire procedure is messy, though fairly straight forward, and it serves little purpose to dwell on it here. Suffice to say that the first term on the L.H.S of (7.6) supplies us with our sought after effective mass m for the fundamental mode as approximately 0.067 times the mass of the shell, or in our case, the flangeless gong. The mass of the entire gong is about 5 kg so that the mass of the flangeless gong is approximately 3.5 kg leaving us with an effective mass of the fundamental mode of approximately 230 g.

The shaker applied a force of approximately 4.4 N per ampere of current and, as it could not take more than 1.8 amps without becoming overloaded, the maximum force it could apply to the gong was $\approx$ 7.9N. Theoretical considerations therefore require values of G, remembering that the fundamental frequency has been normalised to unity, of up to 10^{-4}Nkg^{-1}.

7.9 Computed behaviour for single mode system.

Equation (7.5) was integrated numerically using the Runge-Kutta formula for integration (Rektorys 1969) and time intervals of $\frac{1}{100}\times$ the forcing frequency. The damping we measured is really quite small and the procedure needed to be followed for at least 1000 orbits in order to let the system settle down before observing the resulting state space.

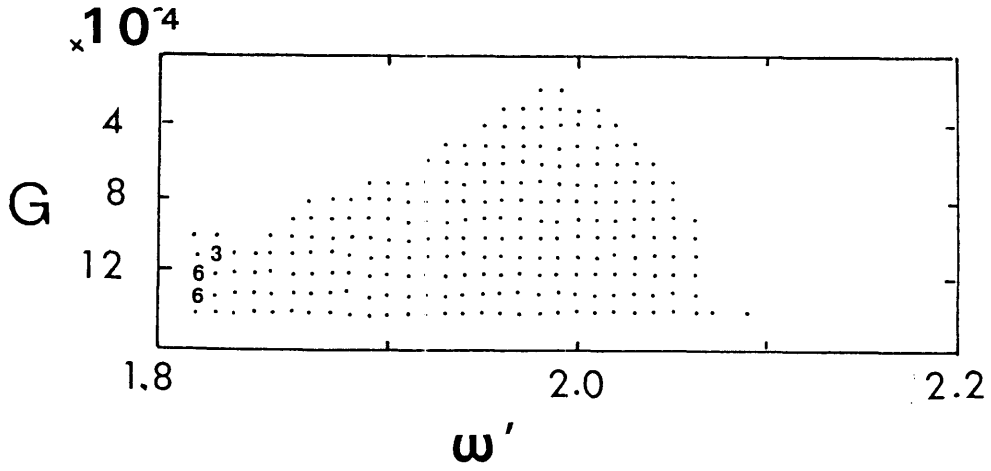

Figure 7.14: Map of G and ω' values which produce bifurcations for the equation $\ddot{x} + 0.014\dot{x} + 253x^2 + 16840x^3 = G\sin\omega' t$. Bifurcation into two points is marked with a dot and into more points with the appropriate number.

The first series of observations were made for a range of values of both G and ω' and supposing the fundamental mode frequency of 96 Hz was the only mode present on the gong. G was varied in steps of 10^{-5} from 10^{-5} to 10^{-4} and then in steps of 10^{-4} from 10^{-4} to 10^{-3}. For values of ω' between 0.96 and 1.05 there appears to be no combination of G and ω' within this range, that, coupled with our values for A, B and k, could produce anything more than a single orbit in state space .

However, if the forcing frequency is about double the mode frequency then, for large forcing amplitudes, driving the mode to an amplitude of up to 1cm, and therefore rather larger than we observed experimentally,the motion was seen to bifurcate so that a subharmonic of half the forcing frequency was driven . The values of G and ω' for which such bifurcations occurred are shown on a map (Fig.7.14) where each grid point is marked with a dot if obvious bifurcation occured and left blank if the motion was purely at the forcing frequency. Fig.7.15(a) depicts the Poincare mapping for bifurcation into two points. Fig. 7.15 (b) shows a splitting into six points.

If a model of the gong as a single mode system can produce such results surely it is worthwhile investigating a more realistic model. In truth we shall need an infinite array of coupled equations to represent the motion of the normal modes of the gong. We shall obviously have to be content with less than this and in fact, we shall find that to construct a model of the gong as a two mode system we need to make a number of simplifing

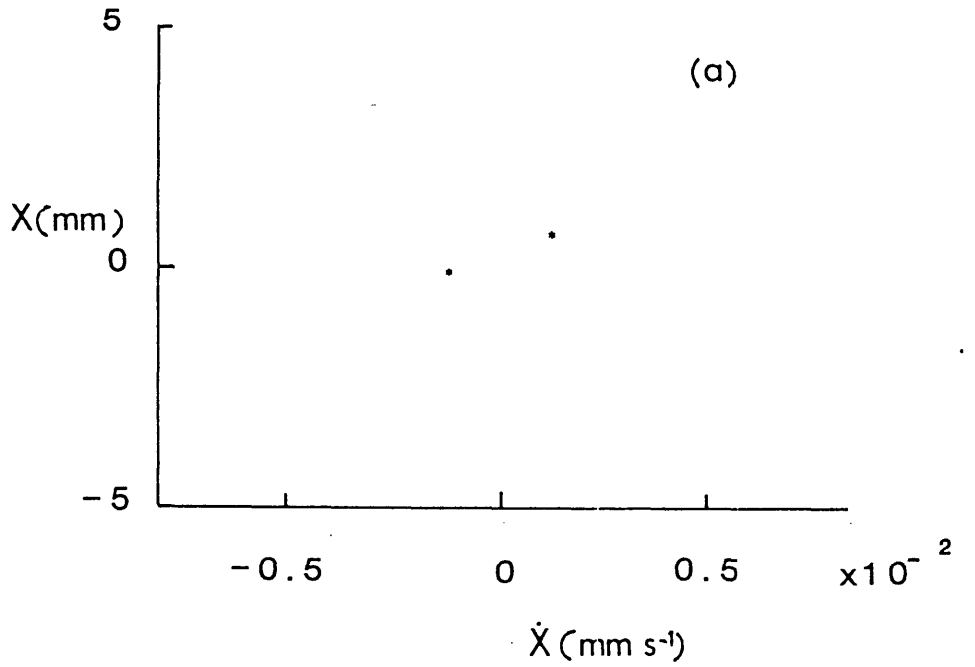

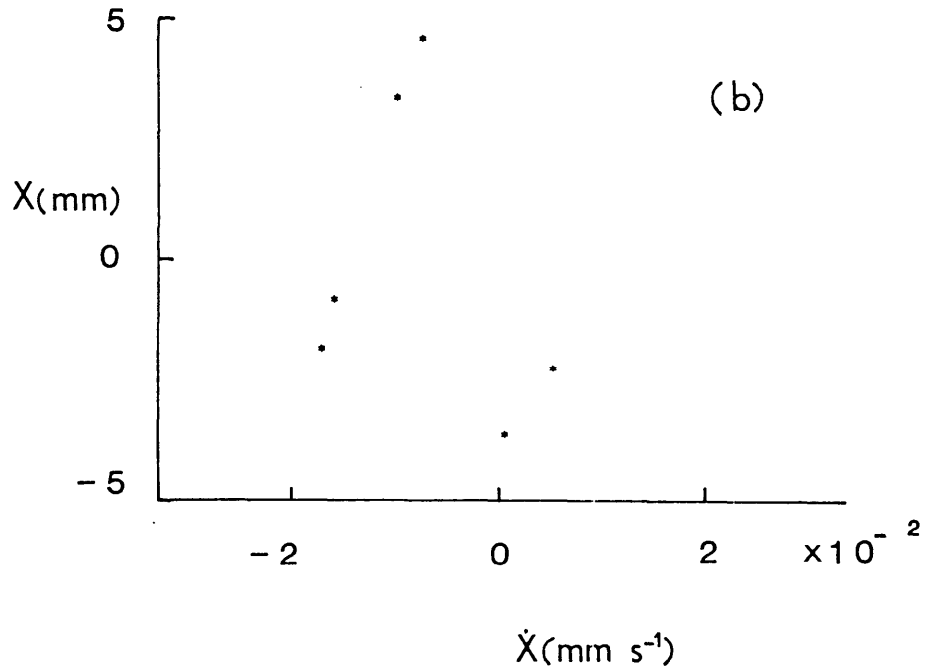

Figure 7.15: Bifurcations ocurring for the equation $\ddot{x} + 0.014\dot{x} + x + 253x^2 + Bx^3 = G\sin\omega' t$ for (a)$G = 0.0004, \omega' = 2.0$ (b)$G = 0.0012, \omega' = 1.8$.

assumptions.

7.10 The gong as a two-mode system.

We write the equation of motion of the two modes in the form of (7.1) with a modification to the third order nonlinear term so as to make it the result of a contribution from tension due now to both modes. Thus we get,

$$\ddot{x_1} + 2k_1\dot{x_1} + n_1^2 x_1 + A_1 x_1^2 + B_1 x_1(x_1^2 + x_2^2) = G\sin\omega t \qquad (7.10)$$

$$\ddot{x_2} + 2k_2\dot{x_2} + n_2^2 x_2 + A_2 x_2^2 + B_2 x_2(x_1^2 + x_2^2) = G\sin\omega t \qquad (7.11)$$

where the parameters n_1 and n_2 are the factors by which the frequency of modes 1 and 2 respectively differ from the fundamental mode, the frequency of which has been normalised to unity.

If we take mode 1 as the fundamental mode of 96 Hz as in the previous model, then $n_1 = 1$ and we have a value for A_1 and B_1 from our previous analysis. Estimates of A_2 and B_2 for n_2 other than 1 will, however, involve far more complex analysis on the motion of modes other than the fundamental. As we are restricting ourselves at this point to merely investigating the effect of a second mode on the response of the first mode we shall, for simplicity, just assume that $A_2 = A_1 = A$ and $B_2 = B_1 = B$ as previously calculated.

7.11 Results for a two-mode system.

Equations (7.10) and (7.11) can now be integrated numerically, again using a Runge-Kutta formulation with 100 time steps per period of the forcing term. Two different situations were investigated this time. The first consisted of a gong with normal modes of frequency at 96 Hz and 196 Hz and the second was for a gong with normal modes at 96 Hz and 180 Hz. Observations were made again for a range of G and ω' values. As with the previous model, there appeared to be no combination of G less than 10^{-4} with ω' that could produce anything more than a single orbit. Fig. 7.16 is a map showing values of G and ω' which were found to produce bifurcation of one or both modes for G up to 10^{-3}.

Interestingly, some of the attractors were more than just single or double points but rather showed rings on their Poincare mapping. These of course do not represent chaos but rather quasi-periodic motion as mentioned in the introduction to chaos in chapter 1. Fig. 7.17 shows an example.

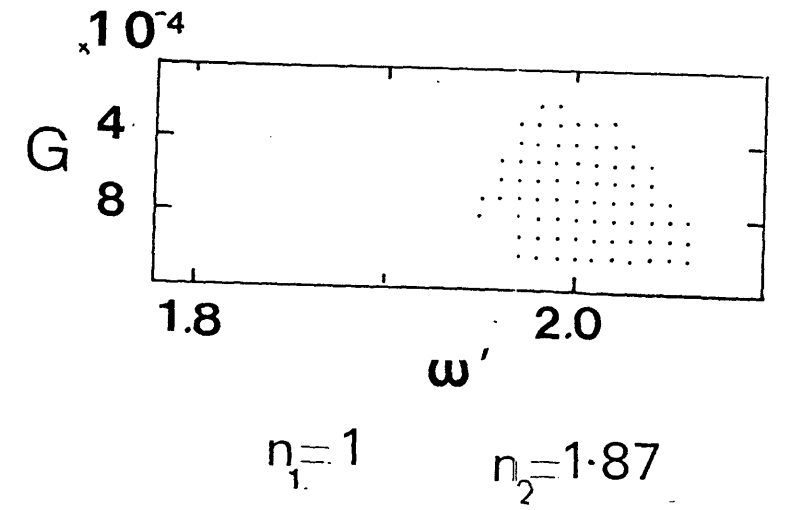

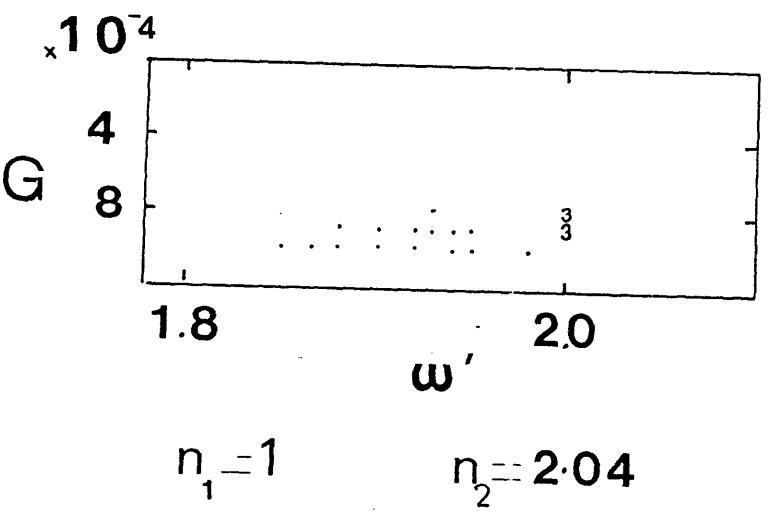

Figure 7.16: Map of values of G and ω' for which the coupled equations (7.10) and (7.11) with $A_1 = A_2 = 253$ and $B_1 = B_2 = 16840$ produce bifurcations. Bifurcation into two points is marked with a dot and into more is marked with the appropriate number.

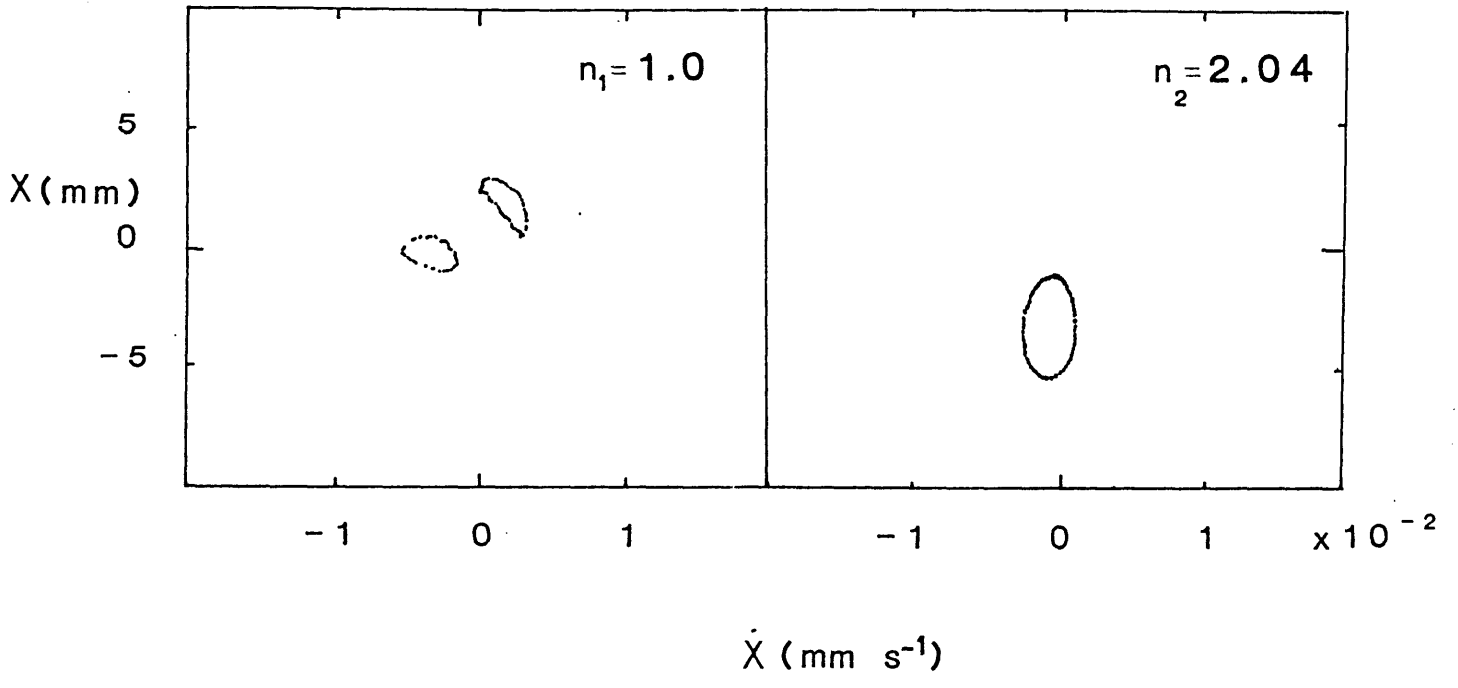

Figure 7.17: Poincare point attractors displaying ring formation for the coupled equations of (7.10) and (7.11) with $\omega' = 1.9$ and $G = 0.0009$.

7.12 Summary of the behaviour of a forced gong.

We have seen that the model of a gong as a single mode system displays bifurcations of its motion for particular forcing frequencies and amplitudes. Furthermore, we have seen that the addition of a second mode to our model can quite radically change the type of behaviour observed. If we then extrapolate these results to consider a true gong with a multitude of normal modes each governed by an equation in the form

$$\ddot{x}_p + 2k_p\dot{x}_p + n_p^2 x_p + A_p x_p^2 + B_p x_p \sum_m x_m^2 = G\sin\omega' t \qquad (7.12)$$

then it is not hard to imagine how bifurcations of some, if not all, the modes could occur. Furthermore, if we include our earlier experimental observations that the forcing of the gong at a particular frequency causes the generation of modes at harmonic frequencies, then we can surmize that the resulting motion is most certainly complex and quite probably chaotic.

7.13 The struck gong.

Let us return now to the original question of the sound produced by a struck gong. Clearly, if there is no external periodic force, we cannot examine the motion in terms of chaos as the attractor will just be a single point at $(x, \dot{x}) = (0, 0)$. It is tempting to investigate the situation when the forcing term $G \sin \omega' t$ in (7.10) and (7.11) is replaced by an impulsive excitation at $t = 0$ and assume that the damping parameters k_n are zero. However, since the value of the damping is critical in determining the presence of chaos, it would not really be furthering our cause to make such an assumption.

Instead, let us look a little more simply at the situation. We integrate (7.10) and (7.11) numerically, this time with the forcing term equal to zero and the initial conditions such that the modes may have particular initial velocities and zero initial displacements, as might be expected for a struck gong.

If we start by assuming that only the fundamental mode ($\nu = 96Hz$) is excited by the strike, then we essentially have a single mode system as there is no way the second mode can be generated from zero initial conditions according to (7.11). Fig.7.18 depicts the extreme displacement of the motion as it changes in time over 2 seconds, for six different initial velocities. We can see that as the size of the initial strike is increased so too, naturally, is the initial amplitude and so, as predicted by Fletcher (1985) (Fig.7.9), the effective centroid of the oscillations becomes more negative. As the amplitude decays with time the centroid of oscillations approaches zero.

If we observe now, the time taken between the peaks in amplitude then we can obtain the results shown in Fig. 7.19 of how the frequency of the mode varies with time for the six different initial strikes. Considering the amplitudes generated, these too reflect the results predicted by Fletcher in Fig.7.9.

If, now, we include the excitation of a second mode by the initial strike, then these results, and we observe in particular the frequency as a function of time, are quite obviously affected by the coupling of the modes (Fig. 7.20), in a manner dependent not only on the initial velocity amplitudes but also on the harmonic relationship between the two modes and their varying damping terms.

Finally let us speculate on the problem of a multimoded system for which many modes are excited by an initial strike. We cannot presume to know exactly what would happen to the frequencies of vibration of any of the modes with their complex couplings but our

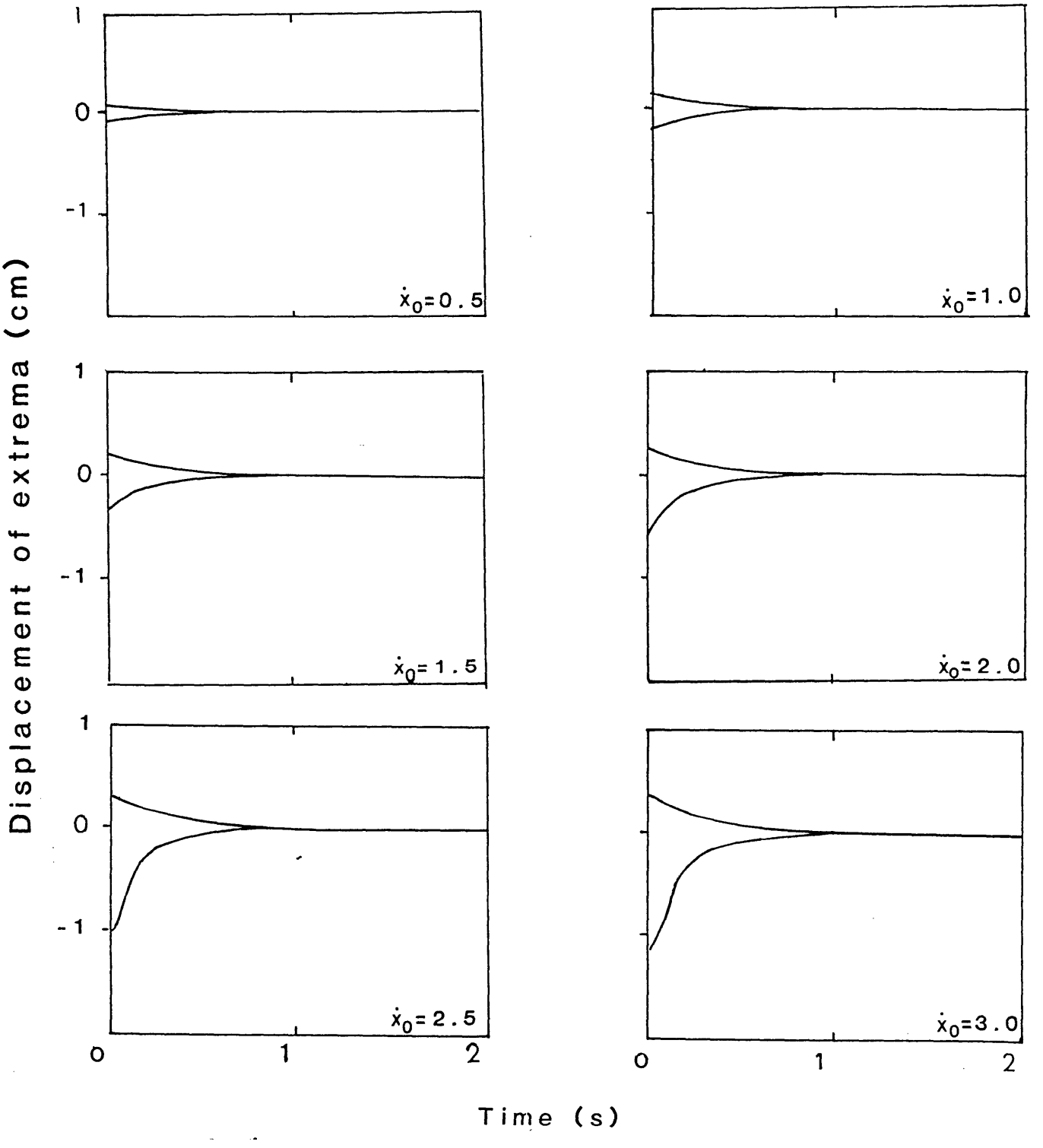

Figure 7.18: Extreme displacement of motion for a struck gong as determined by the equation of motion $\ddot{x} + 0.0014\dot{x} + x + 253x^2 + 16840x^3 = 0$ and the initial velocity as shown.

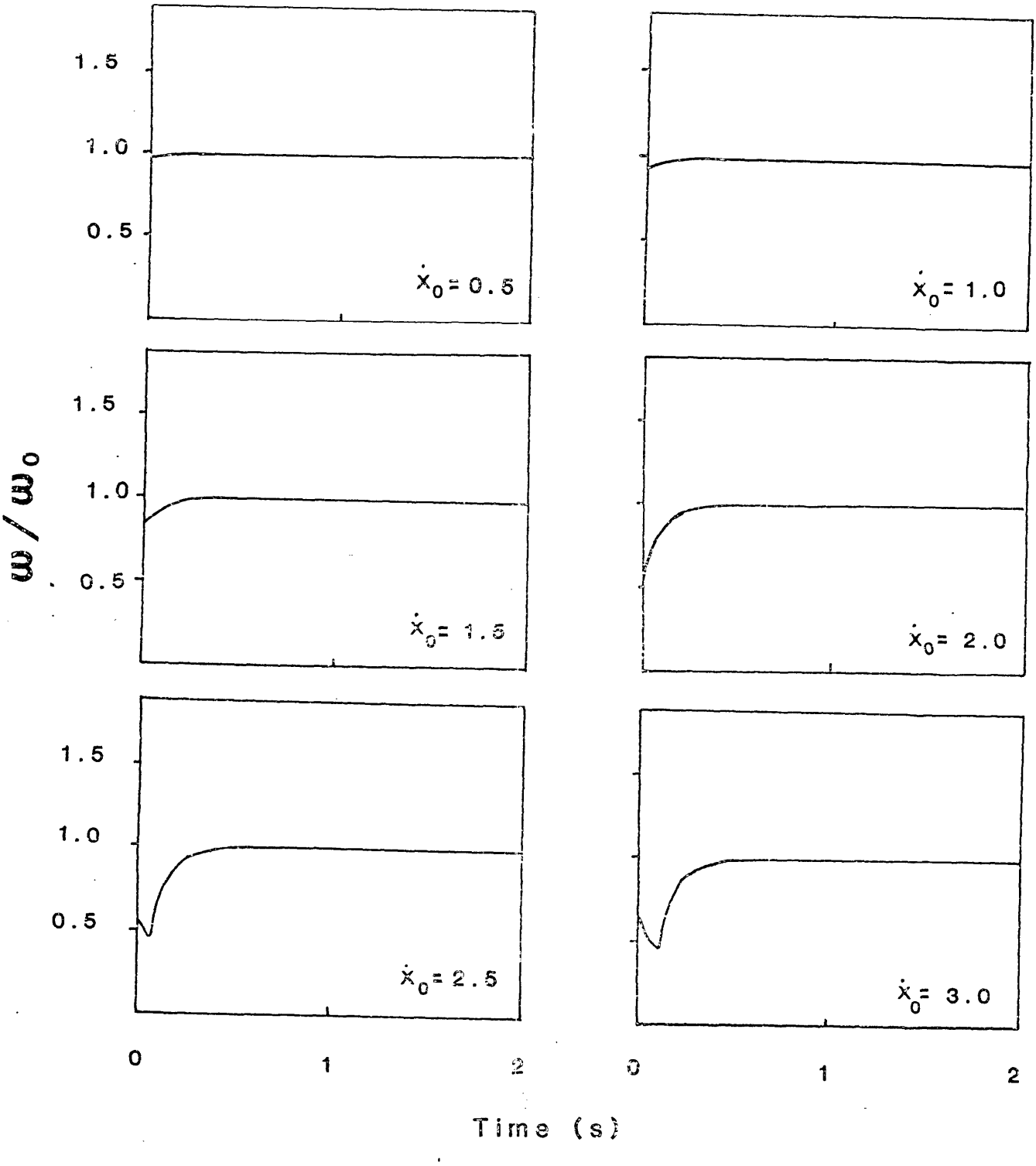

Figure 7.19: Change in frequency with time for a struck gong as determined by the equation $\ddot{x} + 0.014\dot{x} + x + 253x^2 + 16840x^3 = 0$ and the initial velocity as shown.

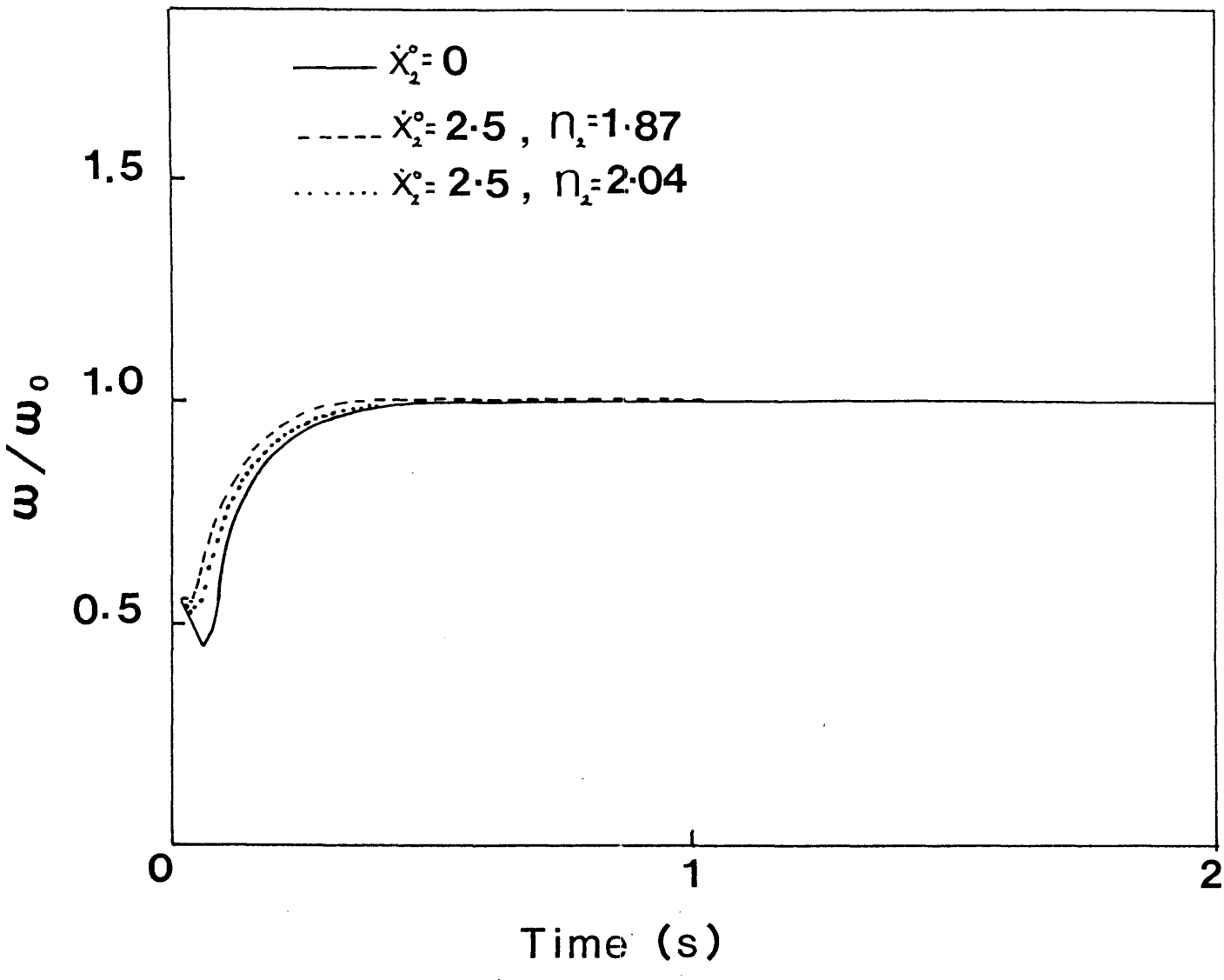

Figure 7.20: Change in frequency with time for a struck gong governed by the equations $\ddot{x_1} + 2k_1\dot{x_1} + x_1 + 253x_1^2 + 16840x_1(x_1^2 + x_2^2) = 0$ and $\ddot{x_2} + 2k_2\dot{x_2} + n_2^2x_2 + 253x_2^2 + 16840x_2(x_1^2 + x_2^2) = 0$ and the initial velocities as shown.

preceeding observations suggest at least that their variation in time for the first second after the strike might not be simple. For a reasonable sized strike the frequencies may change by as much as 50% within 0.5 seconds. If we combine this knowledge with our previous observations of energy cascades to higher harmonic modes due to the presence of the flange around the dome, then it is quite easy to understand how the resulting sound of a struck gong could be initially a fairly harmonic mixture of modes that rapidly changes to, not just a harmonic cascade, but a polyphonic cascade as the initial modes vary in frequency whilst driving their harmonic overtones.

7.14 Conclusion.

In the case of both the string and the kinked bar we have identified the major source of nonlinearity that causes coupling between harmonic modes and have shown, with reasonable experimental confidence, that our identifications were correct. The investigation into the gong has not proved as straight-forward, nevertheless we have managed to gain an insight into the type of behaviour it seems to display. The problem appears to divide into two fairly distinct parts; (i) the struck gong which we originally set out to investigate and (ii) the periodically forced gong which we came across accidently in the course of our experimentation and which proved to be quite fascinating in its own right.

For both the string and the kinked bar the nonlinear techniques used were relatively straight-forward. In the case of the struck gong the problem was complicated by the inclusion of an extra dimension, nevertheless we managed to observe both a harmonic mode coupling as suggested by an extrapolation of our results for the kinked bar, and a considerable change in frequency for the fundamental which could be affected by the presence of other modes. These results together suggest that the sound of a struck gong will build from the initial modes present at the actual strike to a conglomeration of all possible modes of the gong producing a nonharmonic crash within the order of 1 second.

The case of the periodically forced gong led us to include an investigation into chaos. Our rudimentary results, both theoretical and, especially, experimental, strongly suggest that we have here a marvellous example of chaotic motion. However we were trying to investigate a complex mutimoded system with a technique not yet fully understood for single moded systems and our observations were therefore limited. Chaos itself, is proving a fascinating subject to many varied areas of mathematics and physics and maybe, as more

knowledge is gained on why it occurs and how multimoded systems are effected, we may be able to explain more fully the motion of a periodically forced gong. Indeed it requires only a little stretching of the imagination to speculate that further understanding of chaos in general may also enable us to link more closely the behaviour of the forced gong to that of the struck gong.

References

Anand G.V (1969) Large-amplitude damped free vibration of a stretched string. *Jour. Acoust Soc. Amer. 45(5) , p1089-1096*

Carrier G.F. (1945) On the nonlinear vibration problem of the elastic string. *Quart. Appl. Math. 3(2) , p157-165*

Crutchfield J.P., **Farmer J.D.,** **Pakard N.H.** and **Shaw R.S.**(1986) Chaos. *Scientific American 255(6),p 38-49*

Eisley J.G. (1964) Nonlinear vibrations of beams and rectangular plates. *Zeits. Ange. Math. und Physik 15 , p167-175*

Eringen A.C. (1952) On the nonlinear vibration of elastic bars. *Quart. Appl. Math. 9 ,p361-369*

Feigenbaum M.J.(1980) Universal behaviour in nonlinear systems. *Los Alamos Science 1, p4-27*

Fletcher N.H. (1985) Nonlinear frequency shifts in quasisperical-cap shells: Pitch glide in Chinese gongs. *Jour. Acous. Soc. Amer. 78(6) , p2069-2073*

Gough C. (1983) The nonlinear free vibration of a damped elastic string. *Jour. Acous. Soc. Amer. 75(6), p1770-1776*

Grossman P.L., Nonlinear vibrations of shallow spherical shells.
Koplik B. and *Jour. Appl. Mech. , p451-458*
Yu Y-Y(1969)

Harrison H. (1948) Plane and circular motion of a string.
Jour. Acous. Soc. Amer. 20(6), p874-875

Holmes P.(1977) 'Strange' phenomena in dynamical systems and their physical implications.*App. Math. Modelling 1,* p362 - 366

Holmes P. and Strange attractors and chaos in nonlinear mechanics.
Moon F.C. (1983) *Jour. App. Mech. 50 , p1021*

Hoppmann W.H.(1961) Frequency of vibration of shallow spherical shells.
Jour. Appl. Mech., p305-307

Hoppmann W.H and A study of vibrations of shallow spherical shells.
Baronet C.N.(1963) *Jour. Acous. Soc. Amer. 34(8), p1067-1072*

Johnson M. and On transverse vibrations of shallow spherical shells.
Reissner E.(1958) *Quart. App. Math. 25, p367-380*

Kalnins A. (1961) On vibrations of shallow spherical shells.
Jour. Acous. Soc. Amer. 33. p1102 - 1107

Kalnins A. and VIBRATION Beams, Plates and Shells.*Benchmark papers*
Dym C.L. *in Acoustics Vol. 8, Dowden, Hutchinson and Ross Inc. 1976*

Lee E.W.(1957) Nonlinear forced vibration of a stretched string.
Brit. Jour. App. Phys. 8, p411-413

MorseP.(1948) Vibration and Sound.
American institute of physics 1936

Morse P. and **Ingard**(1968) Theoretical Acoustics.
McGraw-Hill 1968.

Murthy G.S. and **Ramakrishna B.S.**(1965) Nonlinear character of resonance in stretched strings.
Jour. Acous. Soc. Amer. 38(3), p461-471

Oplinger D.(1960) Frequency response of a nonlinear stretched string.
Jour. Acous. Soc. Amer. 32(12), p1529 - 1538

Prathap G. and **Pandalai K.A.V.**(1978) On asymptotic solutions to the nonlinear vibrations of curved elements. *Jour. Sound and Vib. 58(3), p463-466*

Reissner E. (1945) Stresses and small displacements of shallow spherical shells [I and II].
Jour. Math. and Phys. 25, p 80-85, 279-300.

Reissner E. (1946) On vibrations of shallow spherical shells.
Jour. Appl. Phys. 17, p1038-1042

Reissner E. (1955) On axi-symmetrical vibrations of shallow spherical shells.
Quart. Appl. Math. 13, p 279-290

Rossing T.D. and **Fletcher N.H.**(1983a) Acoustics of a tam-tam.
Bulletin AAS 10(1), p21-26

Rossing T.D. and **Fletcher N.H.**(1983b) Nonlinear vibrations in plates and gongs.
Jour. Acous. Soc. Amer. 73(1), p 345-351

Rektorys K. (1969) Survey of Applicable Mathematics.
Iliffe Books Ltd. London

Srinivasan A.V.(1966) Nonlinear vibrations of beams and plates. *Int. Jour. Nonlin. Mech. 1, p179-199*

Tongue B.H.(1986) Existence of chaos in one-degree-of-freedom systems. *Jour. Sound and Vib. 110(1), p69-78*

Tongue B.H.(1987) Characteristics of numerical simulations of chaotic systems. *ASME Jour. Appl. Mech. 54(3), p 695-699*

Ueda (1979) Randomly transitional phenomena in the system governed by Duffing's equation. *Jour. Stat. Physics 20(2)*

Papers resulting from this work.

Nonlinear generation of missing modes on a vibrating string. K.A.Legge and N.H.Fletcher *Jour. Acoust Soc. Amer. 76(1), p 5-12*, 1984.

Nonlinear mode coupling in symmetrically kinked bars. K.A. Legge and N.H. Fletcher *Jour. Sound and Vib. 118(1). p 23-34*, 1987.